nature communications

Article

https://doi.org/10.1038/s41467-024-54374-z

Dual receptor-binding, infectivity, and transmissibility of an emerging H2N2 low pathogenicity avian influenza virus

Received: 13 March 2024

Accepted: 5 November 2024

Published online: 19 November 2024

Check for updates

Ju Sun[1,2,7], Tianyi Zheng[2,7], Mingjun Jia[1,2,7], Yanjun Wang[2], Jingru Yang[2], Yun Liu[1,2], Pengyun Yang[1,2], Yufeng Xie[2], Honglei Sun[3], Qi Tong[3], Jiaming Li[2], Jing Yang[2], Guanghua Fu[4], Yi Shi[2,5], Jianxun Qi[2,5], Wenjun Liu[2,5], Jinhua Liu[3], Wen-xia Tian[1] ✉, George F. Gao[2,5,6] ✉ & Yuhai Bi[1,2,5] ✉

The 1957 H2N2 influenza pandemic virus [A(H2N2)pdm1957] has disappeared from humans since 1968, while H2N2 avian influenza viruses (AIVs) are still circulating in birds. It is necessary to reveal the recurrence risk and potential cross-species infection of these AIVs from avian to mammals. We find that H2 AIVs circulating in domestic poultry in China have genetic and antigenic differences compared to the A(H2N2)pdm1957. One H2N2 AIV has a dual receptor-binding property similar to that of the A(H2N2)pdm1957. Molecular and structural studies reveal that the N144S, and N144E or R137M substitutions in hemagglutinin (HA) enable H2N2 avian or human viruses to bind or preferentially bind human-type receptor. The H2N2 AIV rapidly adapts to mice (female) and acquires mammalian-adapted mutations that facilitated transmission in guinea pigs and ferrets (female). These findings on the receptor-binding, infectivity, transmission, and mammalian-adaptation characteristics of H2N2 AIVs provide a reference for early-warning and prevention for this subtype.

Avian influenza viruses (AIVs) pose a threat to public health worldwide[1]. Since the first human-infecting H5N1 AIV was reported in Hong Kong in 1997[2], multiple subtypes of AIVs have sporadically caused human infections, including H9N2, H7N9, H6N1, H10N8, H5N6, H7N4, H10N3, and H3N8[3–10]. Therefore, strengthening AIV surveillance in animals and a public health risk assessment of novel AIVs are imperative for the control and prevention of emerging and re-emerging influenza pandemics and epidemics.

To date, at least five influenza pandemics have been caused by H1N1, H2N2, and H3N2 viruses[10,11]. Among them, the 1957 H2N2 pandemic virus [A(H2N2)pdm1957] emerged in humans through the reassortment between the circulating human H1N1 virus and H2N2 AIVs: the HA, NA, and PB1 gene segments from H2N2 AIVs, while the remaining five gene segments were from the human H1N1 virus[12,13]. The A(H2N2)pdm1957 spread rapidly among humans, causing the "Asian influenza" pandemic. However, it suddenly disappeared after 11 years of circulation in humans when the H3N2 virus emerged in 1968[14]. Over

[1]College of Veterinary Medicine, Shanxi Agricultural University, Jinzhong 030801, China. [2]CAS Key Laboratory of Pathogen Microbiology and Immunology, Institute of Microbiology, Center for Influenza Research and Early-warning (CASCIRE), CAS-TWAS Center of Excellence for Emerging Infectious Diseases (CEEID), Chinese Academy of Sciences (CAS), Beijing 100101, China. [3]National Key Laboratory of Veterinary Public Health and Safety, Key Laboratory for Prevention and Control of Avian Influenza and Other Major Poultry Diseases, Ministry of Agriculture and Rural Affairs, College of Veterinary Medicine, China Agricultural University, Beijing 100193, China. [4]Institute of Animal Husbandry and Veterinary Medicine, Fujian Academy of Agricultural Sciences, Fuzhou 350013, China. [5]University of Chinese Academy of Sciences, Beijing 100049, China. [6]The D. H. Chen School of Universal Health, Zhejiang University, Hangzhou 310058, China. [7]These authors contributed equally: Ju Sun, Tianyi Zheng, Mingjun Jia. ✉e-mail: wenxiatian@126.com; gfgao@zju.edu.cn; beeyh@im.ac.cn

50 years have passed since the spread of the last H2N2 virus identified in humans; hence, preexisting antibodies against A(H2N2)pdm1957 have gradually disappeared from the human population[15]. On the other hand, H2 low pathogenicity AIVs (LPAIVs) are continuously circulating in poultry and mammals worldwide[16–18], possibly allowing the reintroduction of H2 viruses into the human population, with or without needing prior reassortment with other viruses.

The viral surface glycoprotein hemagglutinin (HA), a trimeric class I transmembrane protein that binds sialic acid (SA) receptors to initiate virus infection, is a major determinant of host tropism, pathogenicity, and transmission[19]. Generally, the HA of AIVs preferentially binds avian-type α2,3-linked sialic acid (α2-3-SA) receptor, while human-adapted viruses preferentially bind to the human-type α2,6-linked sialic acid (α2-6-SA) receptor. It has been shown that a switch in receptor-binding preference from avian- to human-type, associated with Q226L and G228S substitutions in the receptor-binding site (RBS) of HA, contributed to the emergence of A(H2N2)pdm1957[20–22].

Here, seven H2 LPAIVs possessing diverse antigenicity compared to A(H2N2)pdm1957 are identified in domestic poultry in China from our long-term surveillance[23–25]. Unexpectedly, one H2N2 LPAIV isolate (Dk/FJ/2021) is found to bind both avian- and human-type receptors. In addition, we find that one A(H2N2)pdm1957 strain (A/Singapore/1/1957) isolated in 1957 also has a dual receptor-binding property, while another strain (A/Korea/426/1968) isolated in 1968 preferentially binds human-type receptor. Both the human influenza strains have L226 and S228 residues, and we find that the residues in the 130-loop of RBS will affect the receptor-binding preference. Furthermore, the adaptation ability, pathogenicity, and transmissibility of the H2N2 LPAIV with human-type receptor-binding ability are assessed in mice, guinea pigs, and ferrets. These results will enrich the genetic and antigenic characteristics, and provide new evidence for understanding the molecular basis of receptor-binding and inter-species transmission of H2N2 influenza virus.

Results

H2Ny AIVs present different genetic and antigenic characteristics from the A(H2N2)pdm1957 strain

Phylogenetic analysis of the HA and six internal genes showed that the A(H2N2)pdm1957 strain fell within the Eurasian lineage, along with H2Ny LPAIVs. The A(H2N2)pdm1957 strain formed a separate lineage from the AIV lineage, and no other A(H2N2)pdm1957-like strain has been identified since 1968 based on virus sequences in public databases. In contrast, H2Ny AIVs have continued to circulate and gradually increased in number in animals, evolving into at least three HA clades: 1961–1998 ($n = 61$), 1999–2009 ($n = 58$), and 2009–2022 ($n = 98$). Our seven H2Ny LPAIV strains belong to the 2009–2022 clade (Fig. 1a and Supplementary Fig. 1). The NA gene of A(H2N2)pdm1957 also formed an independent lineage distinct from the lineages of Eurasian and North American HxN2 AIVs, swine HxN2, and human seasonal H3N2 influenza viruses (Supplementary Fig. 1).

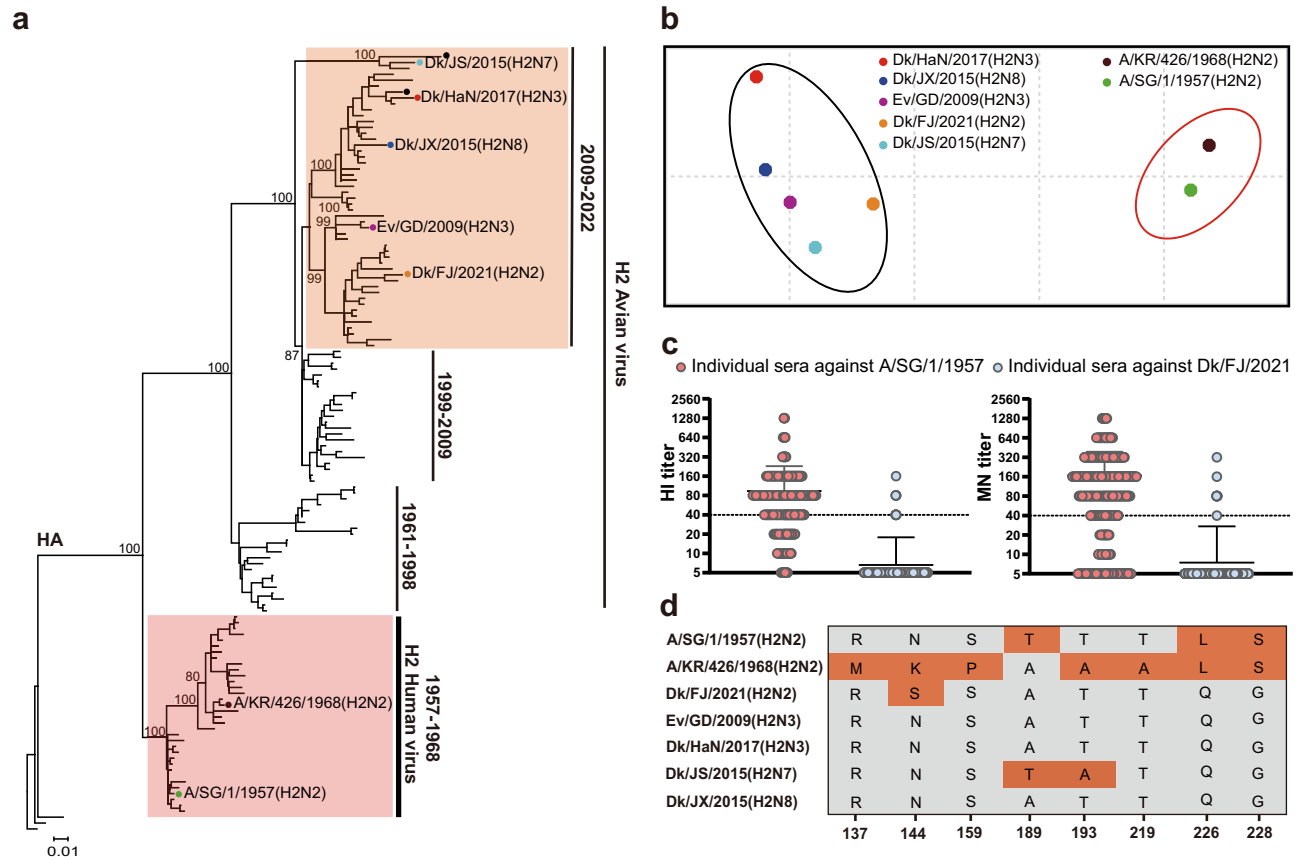

Fig. 1 | Phylogenetic and antigenic characteristics of the H2Ny avian influenza viruses identified in this study. a Phylogenetic tree of the HA gene of H2 influenza viruses. Pink and orange grids represent the H2 human virus lineage and the current circulating H2 avian influenza virus (AIV) lineage, respectively. The dotted viruses in the AIV and human virus lineages are the sequenced H2Ny AIVs and reference human viruses used in this study. **b** Antigenic cartograph representation of the hemagglutination inhibition (HI) data was generated using an antiserum panel. One unit (grid) represents a 2-fold change in the HI assay. H2N2 human viruses are encircled in red oval, while H2 AIVs are encircled in black oval. **c** Individual sera from humans ($n = 419$) born prior to 1968 were examined for antibodies against the H2N2 pandemic strain A/SG/1/1957 and the AIV strain Dk/FJ/2021 by hemagglutination inhibition (HI) and microneutralization (MN) assays. Sera with HI or MN titers ≥ 1:40 are considered positive. Data are represented as the mean ± SD. **d** Sequence alignment of the key residues in the receptor-binding site (RBS) of the HAs from representative H2 viruses.

https://doi.org/10.1038/s41467-024-54374-z

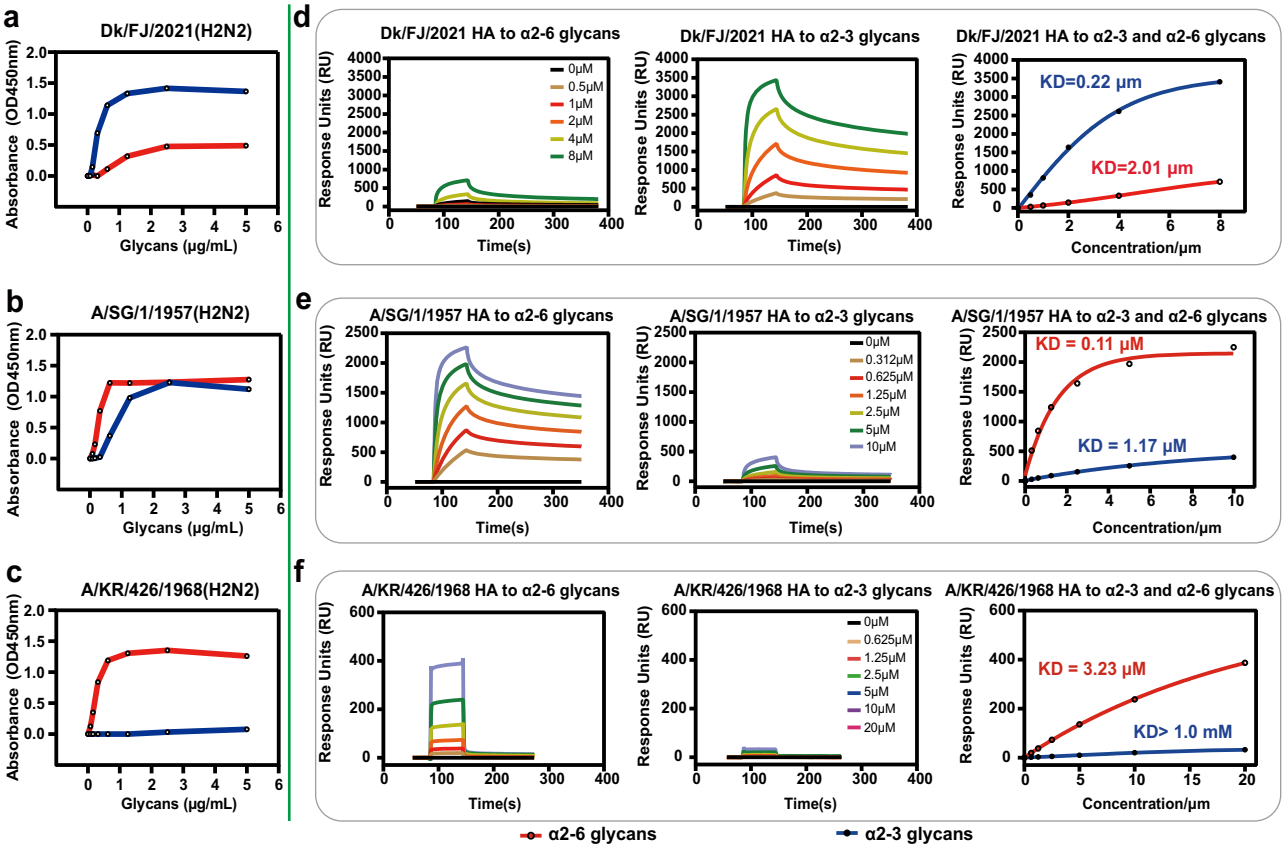

Fig. 2 | Receptor-binding properties of the wild-type H2N2 avian and human viruses. a–c Receptor-binding properties at the virus level. Results of the solid-phase binding assays for Dk/FJ/2021 (**a**), A/SG/1/1957 (**b**), and A/KR/426/1968 (**c**) to both α2,3-linked (3′-SLNLN) and α2,6-linked (6′-SLNLN) sialylglycan receptors. Blue and red lines represent 3′-SLNLN and 6′-SLNLN, respectively. Vaccine strains (A/SG/1/1957 and A/KR/426/1968) were rescued by reverse genetics, in which HA and NA genes from the wild-type A/SG/1/1957 or A/KR/426/1968 strains and the internal genes from the vaccine backbone A/PR/8/34. A/CA/04/2009 and A/VN/1194/2004 were used as controls. **d–f** Receptor-binding properties at the protein level. BIAcore diagram of HAs from Dk/FJ/2021 (**d**), A/SG/1/1957 (**e**), and A/KR/426/1968 (**f**) binding to 3′-SLNLN or 6′-SLNLN. The binding affinity (K_D) values were calculated using the BIAcore 3000 analysis software (BIAcore version 4.1). The binding curve to the 3′-SLNLN is shown in blue, and that for the 6′-SLNLN is shown in red.

The differences in HA lineages between the human A(H2N2) pdm1957 strains and H2Ny AIVs circulating in animals suggest antigenic drift. Therefore, the antigenic relationship between these two lineages was further analyzed using cross-hemagglutination inhibition (HI) and microneutralization (MN) assays. Five out of seven H2 LPAIVs in clade 2009–2022 were isolated and formed an antigenic group. These strains displayed low reaction activities with two A(H2N2) pdm1957 strains, which were identified in 1957 (A/SG/1/1957) and 1968 (A/KR/426/1968) and grouped into another antigenic group (Fig. 1b and Supplementary Table 1). In addition, 419 sera from humans born prior to 1968 were selected for antibody test against the H2N2 pandemic strain A/SG/1/1957 and the AIV strain DK/FJ/2021. A high positive rate was detected for the pandemic strain (77.3% for HI and 70% for MN), while low seroprevalence was found in the avian strain (2.6% for HI and 2.3% for MN) (Fig. 1c). Taken together, these results indicate that the preexisting immunity obtained from the H2N2 pandemic viruses may not completely protect humans against the currently prevalent H2 AIVs in animals.

The different amino acid residues in the antigenic epitopes of the HA protein between these two lineages probably resulted in different antigenicity (Supplementary Table 2). In addition, several substitutions in the RBS of HA were found between our H2Ny isolates and the A(H2N2)pdm1957 strains (Fig. 1d and Supplementary Table 2), which may affect the receptor-binding abilities of these H2 viruses.

Receptor-binding properties of the avian and human H2N2 influenza viruses

Binding to human-type receptor is an important determinant for AIVs to infect human cells. Therefore, we characterized the receptor-binding abilities of our H2 AIV isolates and compared them to the two A(H2N2)pdm1957 strains (A/SG/1/1957 and A/KR/426/1968). At the virus level, most H2 AIV isolates preferentially bound avian-type receptor, as revealed using a solid-phase binding assay, except for one H2N2 AIV strain (Dk/FJ/2021), which possessed a dual receptor-binding ability. However, its affinity to avian-type receptor was higher than the human-type receptor (Fig. 2a). Interestingly, the A(H2N2) pdm1957 strain (A/SG/1/1957) also presented a dual receptor-binding property but with stronger human-type receptor affinity, while the 1968 strain (A/KR/426/1968) preferentially bound human-type receptor (Fig. 2b, c). As controls, A/California/04/2009(H1N1) (A/CA/04/2009) preferentially bound human-type receptor, while A/Vietnam/1194/2004(H5N1) (A/VN/1194/2004) merely bound avian-type receptor (Supplementary Fig. 2).

The receptor-binding properties of H2N2 human and avian viruses were systematically studied at the protein level using a surface plasmon resonance (SPR) assay. The results were similar to those obtained at the virus level. Dk/FJ/2021 HA bound both avian- and human-type receptors, with affinities of 0.22 μM and 2.01 μM, respectively (Fig. 2d). A/SG/1/1957 HA also displayed a dual binding property with affinities of 1.17 μM and 0.11 μM, respectively (Fig. 2e). In

https://doi.org/10.1038/s41467-024-54374-z

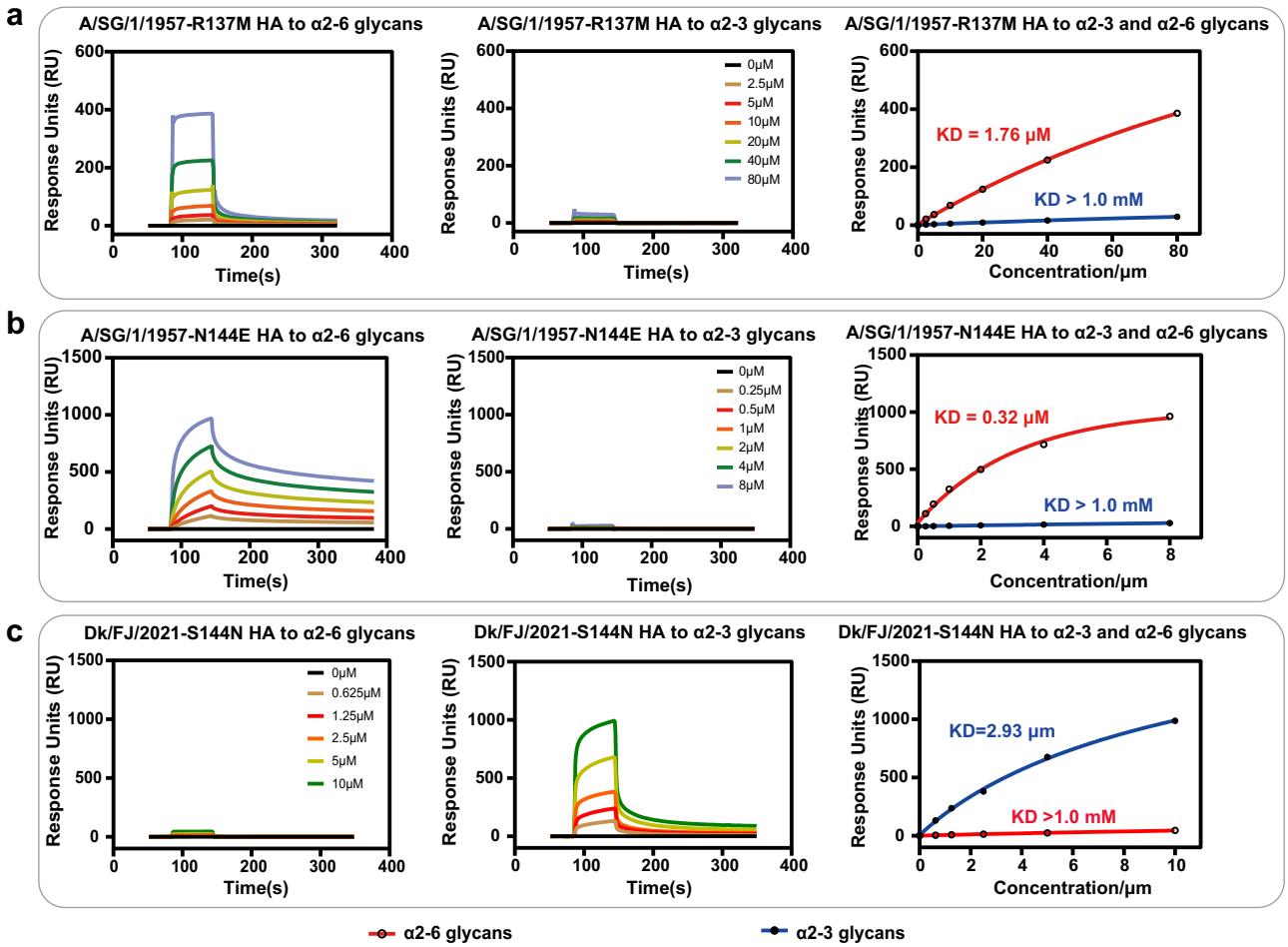

Fig. 3 | Receptor-binding properties of the H2N2 HA mutants. Receptor-binding properties at the protein level. BIAcore diagram of A/SG/1/1957-R137M mutant HA (**a**), A/SG/1/1957-N144E mutant HA (**b**), and Dk/FJ/2021-S144N mutant HA (**c**) binding to 3′-SLNLN or 6′-SLNLN. The binding affinity (K_D) values were calculated using BIAcore 3000 analysis software (BIAcore version 4.1). The binding curve of the 3′-SLNLN is shown in blue, and that for the 6′-SLNLN is shown in red.

contrast, A/KR/426/1968 HA exhibited a preference for the human-type receptor, with an affinity of 3.23 μM (weaker than that of A/SG/1/1957), showing negligible binding to the avian-type receptor (K_D > 1 mM, beyond the SPR measurement range) (Fig. 2f).

Although sharing L226 and S228 on the HA protein, A/SG/1/1957 and A/KR/426/1968 viruses exhibited distinct receptor-binding properties, which may be caused by six residue substitutions in the RBS: R137M, N144K, S159P, T189A, T193A, and T219A (H3 numbering) (Fig. 1d and Supplementary Table 2). So we introduced single substitution of these sites into the A/SG/1/1957 HA protein. The SPR assays showed that a single R137M residue substitution shifted A/SG/1/1957 HA to human-type receptor preference (with an affinity of 1.76 μM, Fig. 3a). However, the other five substitutions (N144K, S159P, T189A, T193A, and T219A) did not affect the dual receptor-binding property of A/SG/1/1957 (Supplementary Fig. 3a–e).

In addition, based on the sequences in publicly available databases, we found that the proportions of R137K and N144E substitutions in the human H2N2 epidemic viruses after 1960 was 54.2% (32/59) and 15.3% (9/59), respectively. Therefore, we also performed these two substitutions in the HA of A/SG/1/1957. Interestingly, the R137K substitution did not affect receptor tropism (Supplementary Fig. 3f). In contrast, the N144E substitution enabled A/SG/1/1957 HA to preferentially bind human-type receptor with an affinity of 0.32 μM (Fig. 3b). Taken together, the R137M or N144E substitutions can change the receptor-binding property of human H2N2 HA from dual receptor binding to a preference for human-type receptor.

Moreover, unlike other H2 viruses, the Dk/FJ/2021 strain possesses N144S substitution in the HA protein (Fig. 1d and Supplementary Table 2). Therefore, we generated a mutant Dk/FJ/2021 HA protein with the S144N substitution and characterized its receptor-binding property using SPR. The results showed that the S144N mutant only bound avian-type receptor (Fig. 3c), indicating that the residue S144 is responsible for the binding of Dk/FJ/2021 to human-type receptor, further emphasizing the importance of the HA 144 site in regulating the binding of H2 viruses to the receptors.

It is well known that the Q226L and G228S substitutions on the HA protein are critical for binding human-type receptor in H2, H3, H4, H5, and H9 subtype viruses[19,26]. To study the synergistic effects of the N144S-Q226L-G228S substitution, we further introduced substitution combinations L226/G228 and L226/S228 into the Dk/FJ/2021 HA protein (S144-Q226-G228). The SPR results showed that both combinations converted the binding preference of Dk/FJ/2021 HA to human-type receptor (Supplementary Fig. 3g, h), indicating that residue L226 is pivotal for the binding of both human and avian H2 influenza viruses to human-type receptor. In summary, R137M and N144E/S can increase the affinities of human-type receptor, and can result in the exclusive human-type receptor-binding ability of the H2N2 virus together with Q226L.

Structure of H2N2 HAs bound to receptor analogs

To understand the molecular mechanisms of the receptor-binding change of H2N2 HAs, we resolved the HA structures of wild-type (WT)

https://doi.org/10.1038/s41467-024-54374-z

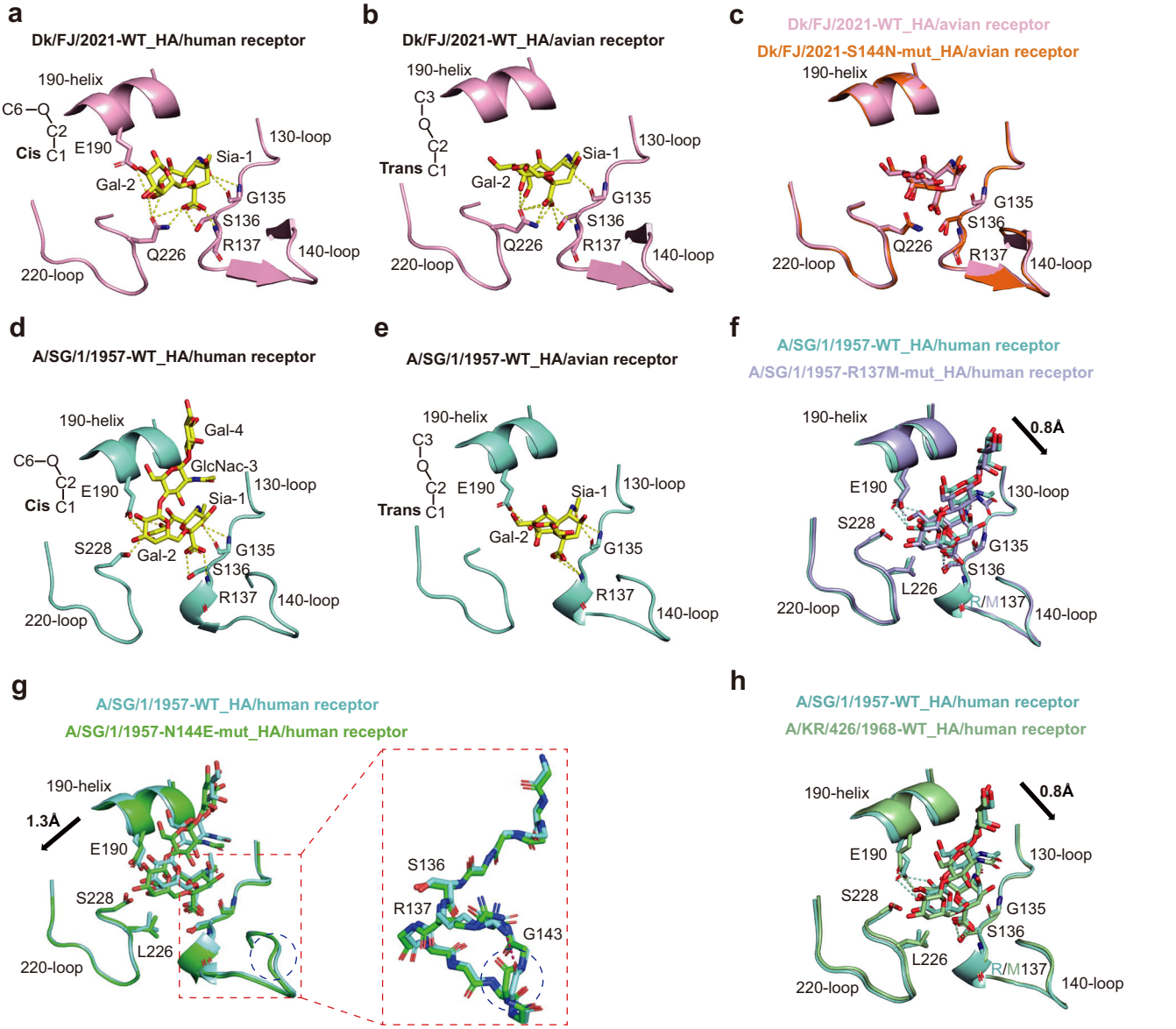

Fig. 4 | Structure basis of the interaction between H2N2 HAs and avian and human receptor analogs. The secondary structural elements of the RBS (130-loop, 140-loop, 190-helix, and 220-loop; H3 number) are labeled in the ribbon representation, together with selected residues in the stick representation. Hydrogen bonds are indicated by the dashed lines. **a**, **b** Molecular interactions of Dk/FJ/2021 wild-type HA with human (**a**) and avian (**b**) receptor analogs. **c** Comparison of the RBSs between the Dk/FJ/2021 HA-avian receptor complex (light pink) and the Dk/FJ/2021-S144N HA mutant-avian receptor complex (orange). A similar trans conformation for glycan binding showed no observable drift between the two complexes. **d, e** Molecular interactions of A/SG/1/1957 HA with human (**d**) and avian (**e**) receptor analogs. **f** Comparison of the RBSs between the A/SG/1/1957 HA-human receptor complex (cyan) and A/SG/1/1957-R137M HA mutant-human receptor complex (lavender). The human receptor analog shifts towards the 130-loop by 0.8 Å in the A/SG/1/1957-R137M complex. **g** Comparison of the RBSs between the A/SG/1/1957 HA-human receptor complex (cyan) and A/SG/1/1957-N144E HA mutant-human receptor complex (green). The human receptor analog shifts towards the 220-loop by 1.3 Å in the A/SG/1/1957-N144E complex. **h** Comparison of the RBSs between the A/SG/1/1957 HA-human receptor complex (cyan) and A/KR/426/1968 HA-human receptor complex (pale green). The human receptor analog shifts towards the 130-loop by 0.8 Å in the A/KR/426/1968 complex.

A/SG/1/1957, A/KR/426/1968, and Dk/FJ/2021, as well as their respective mutants, in complex with two receptor analogs, LSTa (the avian-type receptor) and LSTc (the human-type receptor), using Cryo-Electron Microscopy (Cryo-EM). The resolutions of these structures are shown in the Supplementary Tables 3–5. The complexes exhibited well-defined electron densities for the receptor analogs (Supplementary Fig. 4a–h).

The structure of WT Dk/FJ/2021 HA (S144–Q226) in complex with the human receptor analog LSTc revealed that the analog bound in a cis conformation (Fig. 4a), with ten hydrogen bonds and extensive van der Waals (vdW) interactions between Sia-1 and RBS residues (Supplementary Table 6). The Q226 residue in the RBS formed four hydrogen bonds with Sia-1. Additionally, repulsion between the hydrophobic glycosidic linkage of Sia-1 and Gal-2 in the LSTc and the hydrophilic Q226 residue caused the glycan ring (Gal-2) to be pushed away from the RBS, resulting in only Sia-1 being involved in the interactions with RBS residues (Fig. 4a).

In the complex structure of WT Dk/FJ/2021 HA and avian receptor LSTa, both Sia-1 and other sugar moieties were visible (Supplementary Fig. 4a). Unlike the human receptor analog LSTc, the avian receptor analog LSTa was bound in a trans conformation (Fig. 4b), consistent with observations in the HAs of other AIVs[27]. Notably, the "avian-signature" residue Q226 formed five hydrogen bonds with Sia-1 and one hydrogen bond with Gal-2. Three conserved hydrogen bonds were also

formed between the 130-loop of RBS and Sia-1 (Fig. 4b). This intensive network of hydrogen bonds, complemented by substantial vdW interactions (Supplementary Table 6), collectively contributed to the stabilization of the trans conformation of the avian receptor analog. Hence the WT Dk/FJ/2021 HA can bind both human- and avian-type receptors, and prefers the latter one.

For the complex structure of the S144N-mutant Dk/FJ/2021 HA with the avian receptor analog LSTa, there was no observable drift in the position of the analog compared with the complex structure of the WT Dk/FJ/2021 HA (S144) with LSTa (Fig. 4c). However, the residue S144 appeared to reduce the vdW forces between the 130-loop and 140-loop of the RBS (Supplementary Table 6), resulting in the increased hydrogen bond interactions between the 130-loop and the analog. Taken together, residue S144 enhances the affinity of the HA protein for both avian- and human-type receptors, facilitating the binding of the H2N2 AIV to the human-type receptor.

The complex of the WT A/SG/1/1957 HA (R137-N144-L226-S228) with the human receptor analog LSTc showed that the analog was bound in a cis conformation (Fig. 4d), similar to what has been observed in the HA of the human H3N2 virus. Residue L226 created a hydrophobic environment for the glycosidic linkage between Sia-1 and Gal-2, resulting in the analog adopting a cis conformation. The binding interface also included four hydrogen bonds between Sia-1 and 130-loop, three hydrogen bonds between residue E190 of the 190-helix and Sia-1, and one hydrogen bond between residue S228 of the 220-loop and Sia-1 (Fig. 4d). These hydrogen bonds collectively play a pivotal role in stabilizing the cis conformation of LSTc.

The complex WT A/SG/1/1957 HA with the avian receptor analog LSTa exhibited a strong electron density for Sia-1 and Gal-2 (Supplementary Fig. 4c). Interestingly, in the presence of L226, A/SG/1/1957 HA also bound to the LSTa in a trans conformation (Fig. 4e). Four hydrogen bonds were formed between Sia-1 and the 130-loop, while residue E190 formed a single hydrogen bond with Sia-1. However, no hydrogen bond was observed between the LSTa and the 220-loop, resulting in a weaker interaction, as corroborated by the results of the SPR assay (Fig. 2e).

To figure out the molecular mechanism by which the R137M and N144E substitutions enable A/SG/1/1957 HA to preferentially bind the human-type receptor, we obtained the structures of two mutant HAs (R137M or N144E) in complex with the two receptor analogs. The human receptor analog LSTc adopted cis conformation in both A/SG/1/1957-R137M and A/SG/1/1957-N144E HA mutants (Fig. 4f, g). Comparative analysis showed an obvious shift of the LSTc toward the 130-loop by 0.8 Å for the HAs of A/SG/1/1957-R137M (Fig. 4f) and WT A/KR/426/1968 (Fig. 4h) compared with the WT A/SG/1/1957 HA. Furthermore, an additional hydrogen bond formed between residue S136 and the Sia-1 owing to the repulsion between the side chains of M137 and S136 (Supplementary Table 6). However, as the LSTc repositioned itself, hydrogen bond and vdW interactions between E190 and LSTc significantly diminished (Supplementary Table 6). This phenomenon likely contributed to the reduced affinity of the mutant for both human- and avian-type receptors, thereby explaining the dominant binding to the human-type receptor.

Compared with WT A/SG/1/1957 HA, the human receptor analog LSTc was shifted towards the 220-loop by 1.3 Å for the A/SG/1/1957-N144E mutant HA (Fig. 4g). In addition, in HA-N144E structure, the hydrogen bond between the main chain of G143 (140-loop) and the side chain of R137 (130-loop) disappeared (Fig. 4g). So we assumed that the N-to-E substitution at site 144 attenuated the interactions between the 130-loop and 140-loop, resulting in the side chain of S136 drawing closer to the side chain of L226, which caused the shift of LSTc to 220-loop. The positional adjustments of LSTc further induced the reduction in the interactions of hydrogen bond and vdW between E190 and the analog (Supplementary Table 6). Ultimately, the diminished affinity between HA (E144) and both human- and avian-type receptors resulted in the human-type receptor preference.

Infectivity and dynamic adaptation of the H2N2 AIV strain in mice

The pathogenicity of the Dk/FJ/2021 WT virus was first studied in mice with a dose of 10^6 50% egg-infectious dose (EID_{50}). The infected mice exhibited transient body weight loss compared to the mock-infection mice with PBS (Fig. 5a and Supplementary Fig. 5a). However, the virus replicated well in the lungs of infected mice, as shown in MA1 (Fig. 5a and Supplementary Fig. 5b), suggesting the H2N2 AIV could infect and replicate in mice, a species of mammals, without prior adaptation.

To further study the mammalian adaptation ability of H2N2 AIV and develop a mouse lethal infection model for the pathogenesis study, as well as vaccine and drug development, a series of lung-to-lung passages of the virus were performed in BALB/c mice, and the viruses in each passage were named MA1–MA15. Along with passaging, the body weight losses of the infected mice were gradually aggravated, and all infected mice died at MA14 (Fig. 5a and Supplementary Fig. 5a). The lung viral RNA loads increased after MA3 compared to those in MA1, with relatively higher viral RNA loads starting at MA8 (Fig. 5a and Supplementary Fig. 5b). These results indicate that the replication ability and virulence of the H2N2 AIV in mice gradually increase during the passaging.

To understand the molecular basis of increased virulence acquired after mouse-adapted (MA) passaging, the full genomes of MA1, MA5, MA8, MA10, and MA15 were sequenced using Next-generation sequencing (NGS). We identified two full mutation sites (PB2-E627K and NS1-G183S) that emerged during the passaging and confirmed by Sanger sequencing. The PB2-E627K mutation emerged as early as 5 days post-inoculation (dpi) after WT virus infection (MA1) and was completed in MA5. The NS1-G183S mutation emerged at MA5 and was completed at MA15 (Fig. 5b). In addition, we found that 100% of H2N2 human influenza viruses contained lysine (K) at position 627 of the PB2 gene, whereas most H2 AIVs maintained glutamate (E) at the same position. These results demonstrate that H2N2 AIVs can rapidly adapt to mammals with these mutations, further indicating the potential threat of H2N2 AIV to mammals.

Increased infectivity, pathogenicity, and transmissibility of the H2N2 mutant

To identify the pathogenic characteristics of the H2N2 MA mutant virus, serial virus doses (10^2 to 10^5 EID_{50}) were intranasally (i.n.) inoculated to BALB/c mice. All mice ($n = 5$) died before 8, 7, and 5 dpi in the 10^3 EID_{50}, 10^4 EID_{50}, and 10^5 EID_{50} groups, respectively (Fig. 6a). However, no mice infected with the WT strain died, and only transient body weight loss was observed during the infection with a high dose (10^6 EID_{50}) (Fig. 6a), indicating that the virulence of the H2N2 MA mutant strain in mice is significantly enhanced compared to that of the H2N2 WT strain.

To systematically investigate the pathogenesis of lethal infections in mice caused by the H2N2 MA mutant strain, a comparative infection study between H2N2 WT and MA mutant was performed using a low viral dose of $10^{3.5}$ EID_{50}. The body weights of the MA mutant-infected mice gradually decreased until they died by 7 dpi, while there was no significant decrease in the body weights of the WT group (Supplementary Fig. 6a). In addition, the MA mutant strain induced significantly higher viral RNA loads in the nasal turbinates (~10^8 copies/mL) and lungs (~10^9–10^{10} copies/mL) across the infection at 3, 5, and 7 dpi, as well as the proinflammatory factor secretions (IL-6, MCP-1, IFN-γ, and TNF), and also caused more severe lesions in the lungs based on histopathological changes (Supplementary Fig. 6b–d). The H2N2 MA mutant-infected mice displayed severe pneumonia characterized by alveolar collapse, thickening of the alveolar septa, and severe interstitial inflammatory cell

https://doi.org/10.1038/s41467-024-54374-z

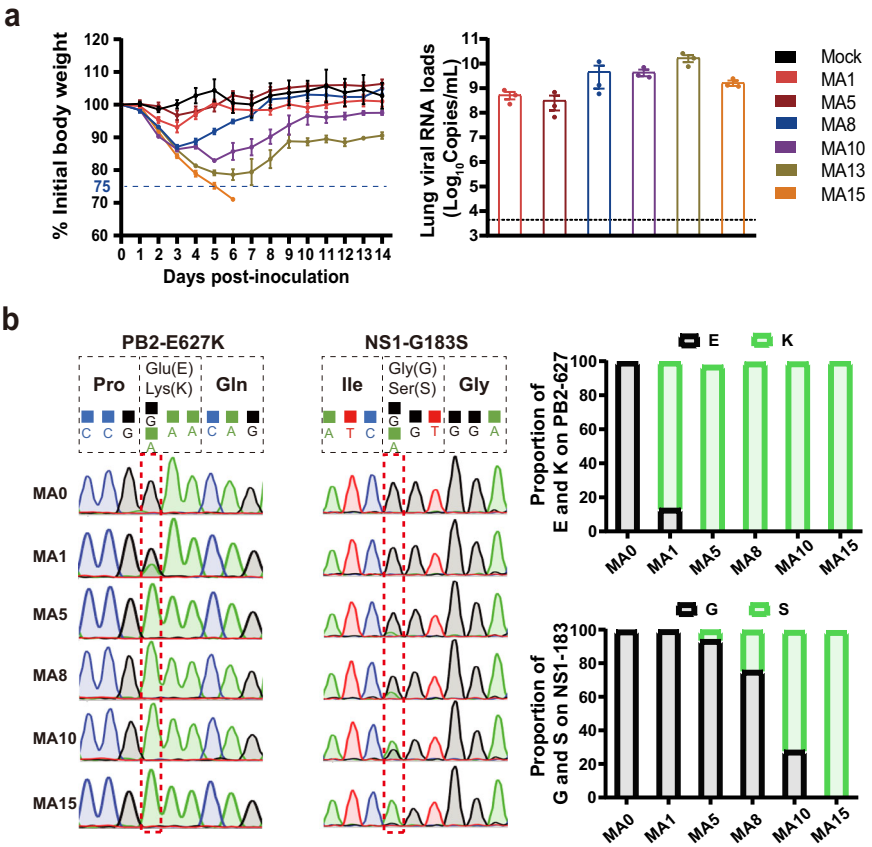

Fig. 5 | Dynamic adaptation of H2N2 avian influenza virus in mice. a 7-week-old BALB/c mice were intranasally (i.n.) inoculated with 10^6 EID_{50} of the Dk/FJ/2021 strain, and then the virus was passaged in mice by lung-to-lung, and the viruses in each passage were named MA1-MA15. The changes in body weight ($n = 3$) and lung viral RNA loads ($n = 3$) of infected mice are shown. The dashed line indicates 75% of the initial body weight or the limit of detection. **b** Dynamic changes of two full mutation sites, PB2-E627K and NS1-G183S, were analyzed using the Sanger sequencing chromatogram and the proportions of amino acids are shown according to the Next-generation sequencing results. The red-dashed boxes show the peaks of nucleotide G and A in the PB2 and NS1 genes.

infiltration. In contrast, mild alveolar collapse and thickening of the alveolar septa were observed in the WT strain-infected mice (Fig. 6b). These results indicate that the virulence of the H2N2 MA mutant strain in mice is higher than that of the WT strain.

The infectivity and replication ability of H2N2 viruses in mammalian cells (MDCK and A549 cells) were also tested in vitro. The MA mutant strain replicated with remarkably higher virus titers (10–100 folds higher) at almost all time points from 12 to 72 hours post-inoculation (hpi) than the WT strain. In A549 cells, the MA mutant strain replicated rapidly with the peak virus titer of $10^{5.09}$ $TCID_{50}$/mL at 72 hpi, versus $10^{4.33}$ $TCID_{50}$/mL for the WT strain (Supplementary Fig. 6e). In MDCK cells, the MA mutant strain also grew faster and reached the peak titer of $10^{5.56}$ $TCID_{50}$/mL at 48 hpi, while the WT strain could not reach the peak titer until 60 hpi with $10^{4.38}$ $TCID_{50}$/mL (Supplementary Fig. 6f). Additionally, to simulate the infection of human respiratory tract by the H2N2 viruses, both WT and MA mutant strains were used to compare their infectivity ability in the primary normal human bronchial epithelial (NHBE) cells. Only 6.3% ± 0.3% of NHBE cells were infected by the WT strain; however, the significantly higher proportion of cells (19.5% ± 0.5%) was infected by the MA mutant strain (Fig. 6c).

These results indicate that the H2N2 MA mutant with PB2-K627 and NS1-S183 has an obvious advantage in infecting in mammalian cells and mice. PB2-E627K mutation could partly contribute to the increased replication ability in mammalian cells and virulence in mice, which has been solidly confirmed in H7N9 and some other AIVs[28,29]. In addition, NS1 protein of influenza A virus could inhibit host innate immunity, enabling virus replication in the infected cells, and also could affect virus virulence in mammals[30]. To study the biological function of the newly identified NS1-G183S mutation, IFN-β secretions from the lungs of infected mice and human A549 cells were tested. In contrast to the significantly higher proinflammatory factor secretions in H2N2 MA mutant-infected mice, IFN-β levels were obviously lower than those of the WT group throughout the infection (Fig. 6d). Similar results were also observed for the WT- and MA mutant-infected human A549 cells at 12, 18, 24, and 30 hpi (Fig. 6e). Furthermore, the strong inhibition activity of NS1-G183S against IFN-β expression was further confirmed in human 293 T cells by transfecting NS1 expression plasmids (NS1-G183 and NS1-S183). Compared with the positive control group, the IFN-β expression levels in the NS1-G183-transfected group and the NS1-S183-transfected group decreased at approximately 3-fold and 13-fold, respectively, at 12 hpi after induction with the Sendai virus (Fig. 6f). These results indicate that host innate immunity is remarkably inhibited by the H2N2 mutant with the NS1-G183S mutation, which probably contributes to increased virus infectivity in human cells and pathogenicity in mice.

The transmissibility of H2N2 AIVs was also evaluated in guinea pigs and ferrets. Three guinea pigs and two ferrets in each group were i.n. inoculated with 10^7 EID_{50} of the WT or MA mutant strains, and direct contact (DC) and respiratory droplet exposure (RD) animals were placed in the corresponding cages at 1 dpi. Nasal washes were collected every two days after the initial infection for virus titration. Both the WT and MA mutant strains replicated well in the infected guinea pigs and ferrets; the viral RNA loads were higher in the MA group than in the WT group in each animal model (Fig. 7a, b). The viral RNA loads of all MA-infected guinea pigs (3/3) were consistently at

https://doi.org/10.1038/s41467-024-54374-z

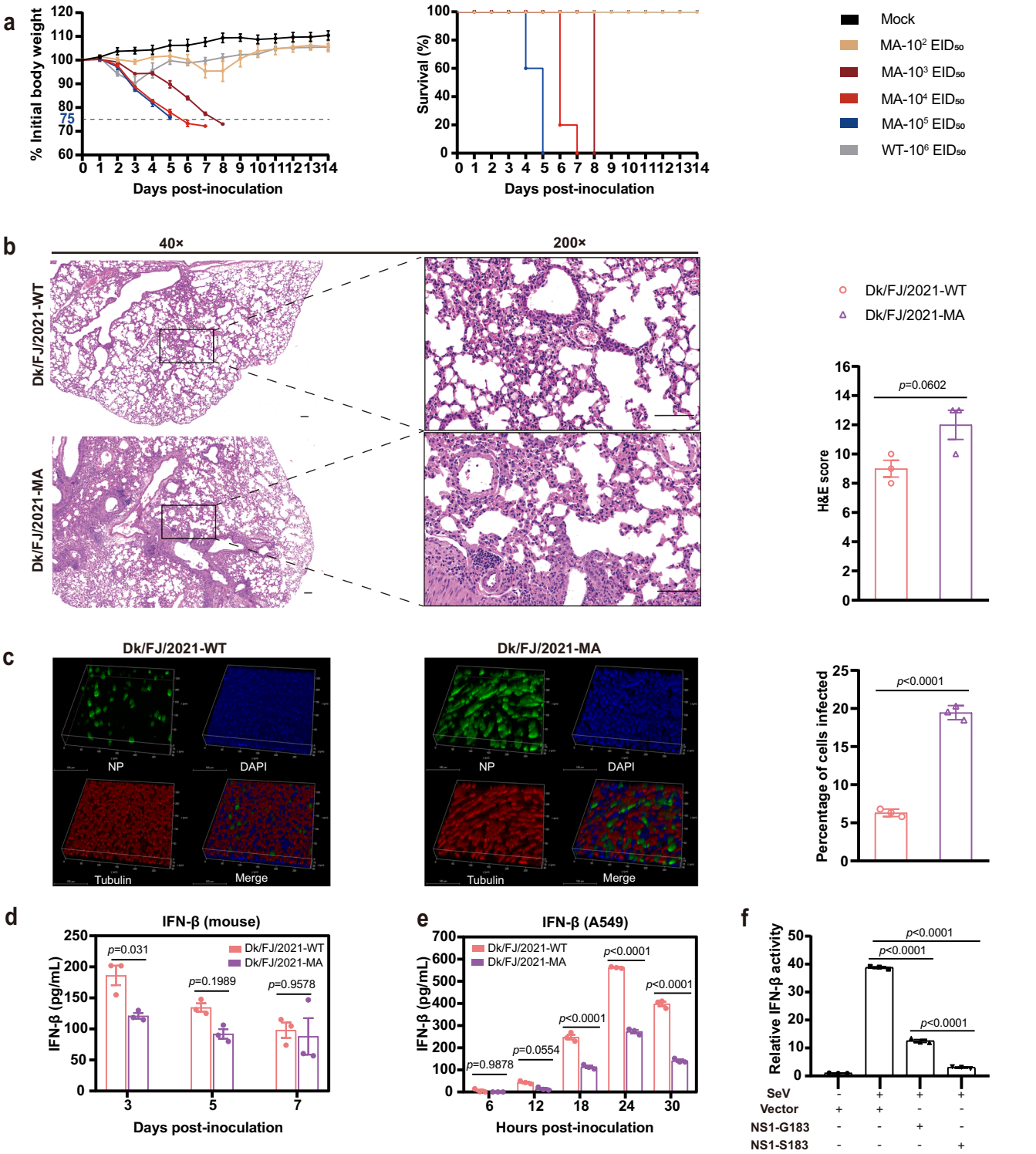

$\sim 10^7$–10^8 copies/mL from 2 to 4 dpi, where the viral RNA loads could also be detected in one animal at $\sim 10^6$ copies/mL at 6 dpi. In contrast, the virus in the WT strain-infected guinea pigs could only be detected at 2 and 4 dpi, with viral RNA loads of $\sim 10^6$–10^7 copies/mL (Fig. 7a). All the MA- and WT-infected ferrets (2/2) shed the virus until 10 dpi, and the viral RNA loads in the MA group were higher than those in the WT group at each detection time point, except at 10 dpi (Fig. 7b). Ferrets infected with either MA or WT strain showed no significant body weight loss (Fig. 7c). These results indicate that, compared to the WT strain, the H2N2 MA mutant strain possesses higher replication ability not only in mammalian cells and mice but also in guinea pigs, and ferrets.

For the DC animals in the WT virus-infected group, the viral RNA was detected in only one DC guinea pig, and no viral RNA was detected in the DC ferret; however, the viral RNA was detected in 2/3 DC guinea pigs and 2/2 DC ferrets in the MA mutant group. No viral RNA was detected in any of the RD animals in the WT group. However, the viral RNA was detected in 2/3 RD guinea pigs and 2/2 RD ferrets (Fig. 7a, b), indicating that the H2N2 MA mutant strain could transmit in ferrets and guinea pigs by respiratory droplet.

https://doi.org/10.1038/s41467-024-54374-z

Fig. 6 | Pathogenicity of the H2N2 avian influenza virus. a Groups of five mice were i.n. inoculated with the Dk/FJ/2021 wild-type (WT) and mouse-adapted (MA) mutant viruses at doses from 10^2 to 10^6 EID_{50}, and the body weight changes and survival rates were monitored for 14 days. The dashed line indicates 75% of the initial body weight. **b** The lungs of mice infected with the indicated viruses were collected at 5 dpi. Lung sections were stained with H&E, and one representative result was shown. The histopathological scores ($n = 3$) were measured. Scale bar, 100 μm. **c** Three-dimensional image of the NHBE cells infected by WT and MA mutant strains with 10^6 EID_{50} at 12 hpi. The viral NP protein (green) was detected by indirect immunofluorescence, ciliated epithelial cells were detected with anti-β-tubulin IV antibodies (red) and cell nucleus were immunostained with DAPI (blue). Percentages of influenza NP-positive cells per DAPI-positive cells were calculated. Data are expressed as mean ± SEM of three randomly selected fields. **d** Mice ($n = 3$) in each group were euthanized at 3, 5, and 7 dpi, and the lung suspensions were used for IFN-β detection. Data are shown as mean ± SEM. **e** Supernatants of A549 cells infected with indicated viruses were collected to determine IFN-β at 6, 12, 18, 24, and 30 hpi. Data are shown as mean ± SEM of three replicates. **f** The NS1 (G183 or S183) expression vector together with the plasmids of IFN-β with luciferase reporter and the internal reference of Renilla luciferase reporter were co-transfected into HEK293T cells. At 24 h post-transfection, the cells were stimulated with Sendai virus for 12 h. The cell lysates were then collected and luciferase activity was measured. Data are shown as mean ± SEM of three replicates. Statistical significance was based on Student's t test and one-way or two-way ANOVA. $p < 0.05$ was considered to indicate statistical significance, and p values are shown on the graphs.

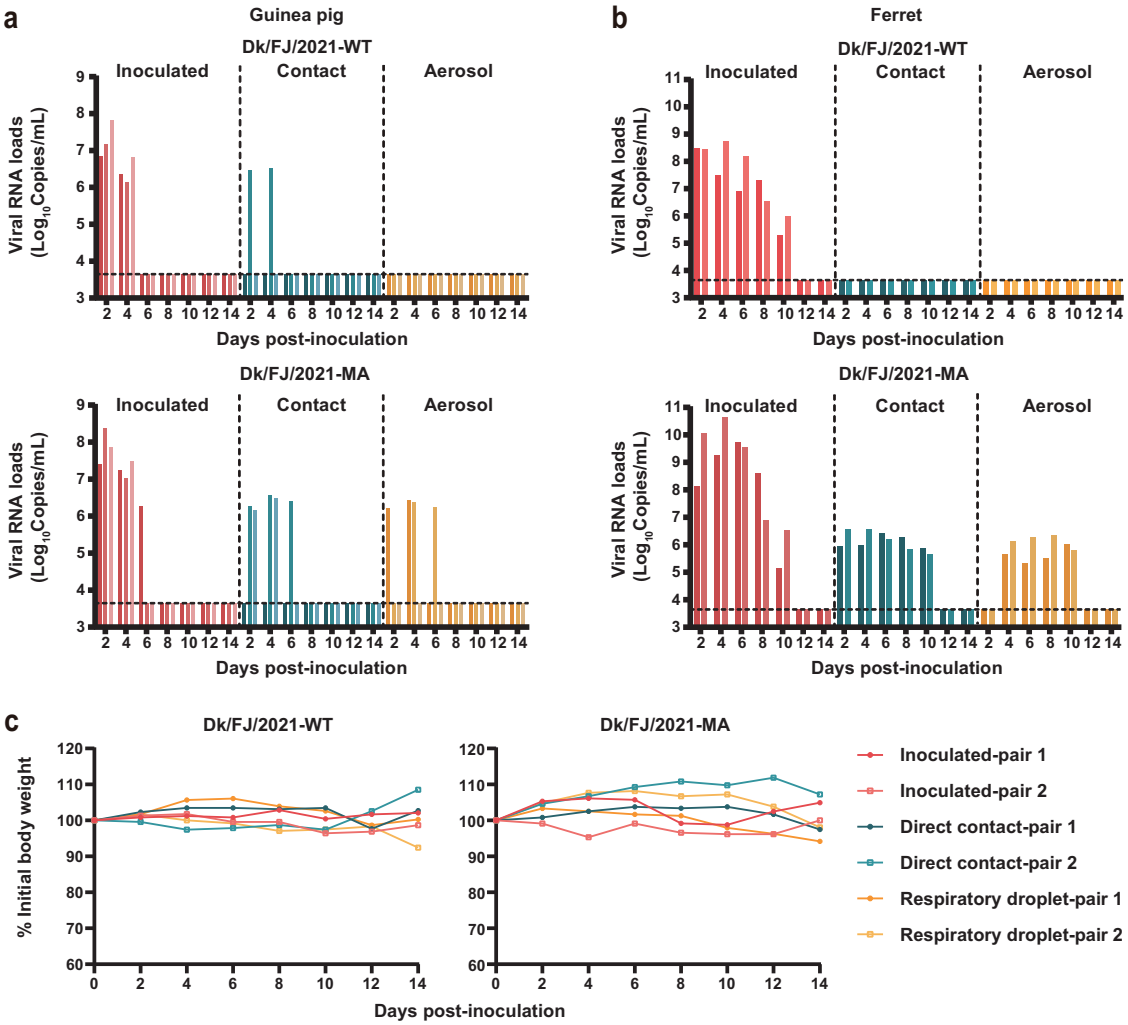

Fig. 7 | Transmission of the H2N2 avian influenza virus. a, b Groups of three guinea pigs (**a**) and two ferrets (**b**) were i.n. inoculated with the WT and MA mutant viruses at a dose of 10^7 EID_{50}. The direct contact (DC) and respiratory droplet exposure (RD) animals were housed in the corresponding cages at 1 dpi. Nasal washes were collected every two days from all animals to detect viral RNA loads. **c** The body weight changes of ferrets ($n = 2$) in the inoculated, DC, and RD groups were monitored for 14 days. The dashed line indicates the limit of detection.

Taken together, lethal infection caused by the H2N2 MA mutant strain in mice is associated to the severe inflammatory damage, expressed as the significant histopathological changes and the proinflammatory cytokine secretions, which is probably induced by the cascade reactions of the suppression of host innate immunity and efficient virus replication in mammalian cells, separately caused by the NS1-G183S and PB2-E627K mutations in the H2N2 virus. This also contributes to the transmission of the H2N2 MA mutant strain in mammals.

Discussion

H2Ny AIVs are continuously circulating in poultry, and it is necessary to assess the risks of introduction of these viruses into mammals and even humans. The circulated H2Ny AIVs have diverged from the A(H2N2)pdm1957 strain in terms of genetic and antigenic characteristics (Fig. 1a, b). Meanwhile, the antigenic change was observed between the H2N2 human viruses from early and late in the epidemic. The A/SG/1/1957 and A/KR/426/1968 strains displayed the antigenic distance with one antigenic unit based on the cross-HI and -MN results,

while there were about 4–6 antigenic units between the other 1957 strains and 1968 strains tested in the previous studies[31,32]. This deviation is likely caused by the different strains used in our study, as the pair of viruses possesses a closer genetic relationship with more similar antigenic sites on HA than those of the other pairs of strains tested before[31–33].

To overcome host barriers, influenza A viruses should be able to bind receptors on the surface of new host cells[19]. In the present study, several H2Ny LPAIVs were identified, where one WT H2N2 AIV (Dk/FJ/2021) possessed the ability to bind both avian- and human-type receptors but preferred to avian-type receptor. Interestingly, the A(H2N2)pdm1957 strain identified in 1957 also had dual receptor-binding property, whereas the 1968 strain preferentially bound human-type receptor (Fig. 2b, c), indicating an adaptation process of the emerging H2N2 virus in humans. The human adaptation process of the 1968 H3N2 influenza pandemic virus also exhibits the similar characteristics. HA from an early human H3N2 isolate could bind both avian- and human-type receptors, then evolved into the specific affinity to human-type receptor during the adaptation[34,35]. For H2 subtype, the Q226L and G228S substitutions might increase the binding affinity of the virus to human-type receptor and reduce binding to avian-type receptor[22,36,37]. Further the present study showed that either the R137M or N144E substitution in the HA protein regulated the binding ability of A(H2N2)pdm1957 to shift from both avian- and human-type receptors to human-type receptor only, and that the N144S also supported the binding of H2N2 LPAIV to human-type receptor (Fig. 3a–c), revealing a new regulation mechanism for the human-type receptor binding of H2 influenza viruses.

Based on their receptor-binding ability, H2N2 AIVs can potentially infect humans and increase their infectivity and pathogenicity upon infection and circulation in mammals or humans. We further evaluated the replication and adaptation abilities of H2N2 AIVs, the second step for novel AIVs to cross-species infect mammals or humans[23]. The WT H2N2 AIV used in this study replicated well and rapidly adapted to mice with two complete mutations, PB2-E627K and NS1-G183S, which resulted in an H2N2 mutant with high pathogenicity in mice and robust replication ability in vivo and in vitro.

The PB2-E627K substitution has been identified as a virulence and host range determinant of influenza viruses in mammals[38–41]. This mutation enhanced the viral polymerase activity in mammalian cells, replication ability in vitro and in vivo, and the virulence in mammals[9,37,42,43]. Further studies found that PB2-E627K mutant allows the AIV RNA polymerase to interact with human acidic nuclear phosphoprotein 32 (ANP32), enabling efficient viral RNA and viral replication in human cells[44,45]. In the present study, the PB2-E627K mutation emerged at 5 dpi in MA1 with 86.4% K residue at the amino acid position 627 (Fig. 5b), as fast as the H7N9 AIV did that we observed in vivo with fine genetic tuning events[28,41], indicating the rapid adaptation of H2N2 AIV to mammals.

Meanwhile, the other mutation site, NS1-G183S, appeared in M5 with ~5.7% S residue, which subsequently evolved into complete residue substitution of S in MA15, synchronous with the gradually increasing virus virulence in mice (Fig. 5a). This suggests that the NS1-G183S mutation may play a role in the virulence of H2N2 AIVs in mammals, which need to further study. Previous studies showed that the NS1 protein of the influenza virus can limit type I IFN production by counteracting RIG-I activation or binding to CPSF30. Among them, the effector domain on NS1 (amino acids 88–202) is key for interacting with the CPSF30 protein to prevent the processing of newly synthesized mRNAs, including IFN-β, which inhibit host innate immunity to promote influenza virus infection[46,47]. However, the NS1-G183S substitution has not been identified before, and its biological function remains unknown. Therefore, we determined the levels of INF-β in vitro and in vivo after infection with the H2N2 WT and MA mutant (with PB2-E627K and NS1-G183S), as well as after transfecting the NS1 plasmid containing the G183S mutation in human cells (Fig. 6d–f). All results showed that the NS1-G183S mutation significantly suppressed the innate immune response (INF-β expression), together with the sharply increased of pro-inflammatory factors, resulting in immune injury and lethal infections in mice, consistent with previous studies on H7N9 AIVs and the SARS-CoV-2 viruses in animal models and humans[28,48,49]. The repressed innate immune response induced the higher replication titers in the infected cells and guinea pigs and ferrets. However, the lung viral RNA loads were not synchronous increasing with the NS1-G183S mutation of the virus during passaging in mice, potentially caused by the defective-interfering (DI) particles that naturally occur during virus infections and also affect virus replication[50,51].

The regulatory mechanism of NS1-G183S in innate immunity and its relationships with viral infection-induced cytokine storm warrant further study, as well as the synergic effect of the NS1-G183S and PB2-E627K mutations on the pathogenic mechanism of H2N2 and other influenza viruses in mammal hosts. In addition, several incomplete mutations with mixed amino acid residues were observed in the virus genes during passaging in mice (Supplementary Fig. 5c), which may also contribute to the increased pathogenicity of the H2N2 AIV in mammals. An example of this is PB2-T271A, which has been reported to be associated with enhanced polymerase activity for the H1N1 pandemic virus (A/CA/04/2009) in mammalian cells[52]. In addition, the incomplete substitutions in HA protein (D41N, G225E, and P324H) were also found in all the MA mutant infected ferrets including the inoculation, DC, and RD transmission groups. Furthermore, the incomplete mutation of G228S was observed in the DC and RD ferrets except of the inoculated animals. The G225E substitution in HA enabled the Eurasian avian-like H1N1 swine influenza virus to transmit in guinea pigs[53]. The G228S substitution was responsible for the switch in receptor specificity and might increase the binding affinity of the human-infecting H3N8 virus to the human-type receptor[9]. All these mutations might facilitate the transmission of the H2N2 AIV in mammals, in which the exact biological functions are worth studying in the future.

The efficiency of viral transmission between humans, whether through direct contact or via airborne routes, is a crucial factor determining the occurrence of epidemics or pandemics[54]. To date, H1N1 and H3N2 human influenza viruses are known to be transmitted between humans via the airborne route, causing annual seasonal influenza. Moreover, multiple AIVs such as H3N8, H5N1, H7N9, and H10N3 have caused sporadic human infections in the past[10]. Compared to human seasonal influenza viruses, these AIVs exhibited limited transmission in mammalian models[9,55–57]. In addition, the circulating H2N2 LPAIV isolate could not transmit between ferrets or guinea pigs via direct contact or respiratory droplets (Fig. 7a, b), which is similar to the previous report[58]. Meanwhile, the positive control virus (A/CA/04/2009) transmitted in all animal groups tested, and negative control virus (A/VN/1194/2004) did not transmit among any animal groups tested. Other previous studies also found that avian H2N2 viruses were only transmitted through direct contact but not via airborne transmission between ferrets[33,36]. Although the tested AIV strains are different, these findings suggest that the circulating H2N2 LPAIV has low transmissibility in mammals including humans. Furthermore, ferrets and guinea pigs infected with either MA or WT strain showed normal appetites and activities without any clinical signs of disease, such as no significant body weight loss in the infected ferrets (Fig. 7c), which is similar to the previous studies using other H2N2 AIVs[33,58]. However, ferrets infected with human H2N2 viruses exhibited mild clinical symptom, including a minor reduction in activity and fever[59]. In addition, in the MA-infected guinea pig group, the viral RNA loads were detected in two RD animals at different time points (2–4 dpi and 4–6 dpi, respectively) (Fig. 7a). The first infected animal was infected via respiratory droplets, while the other animal might be infected either via respiratory droplets or direct contact with the first infected animal.

Ferrets, the best model for influenza research, can more closely simulate the virulence, replication ability, and transmissibility of influenza viruses in humans[33]. Hence, these results suggest that although the MA strain is virulent in mice and can transmit in guinea pigs and ferrets, its pathogenicity to humans could be low, similar to the circulating H2N2 LPAIVs.

In addition, the HA acid stability also affects influenza virus transmission. Several amino acid substitutions on HA, such as T224I and E74D (HA_2) in H10N7 AIV and N210S in H1N1 swine influenza virus, have been identified to enhance airborne transmission efficiency in ferrets[60,61]. In this study, we did not find these known substitutions in the HA protein, while two incomplete mutations (V204M and V552I) were identified during the virus adaptation. The biological functions of these two identified substitutions, particularly their impact on the HA acid stability, need further investigation.

At least three conditions must be met for the emergence of an infectious disease pandemic: a highly transmissible pathogen is pathogenic to humans, and humans lack preexisting immunity against the novel pathogens[62]. Although population immunity against circulating H2Ny AIVs is absent, and the WT H2N2 LPAIV has demonstrated its ability to infect and replicate in various mammalian hosts, it has low pathogenicity and a lack of transmissibility among mammals. This suggest that the risk of circulating H2N2 LPAIVs to cause epidemics or pandemics should be low. However, the H2N2 LPAIV strain just acquired limited mutations that enhance the virulence in mice and enable transmission between mammals. Hence, close epidemiological surveillance and characterization of H2 LPAIVs, as well as the development of vaccines and drugs using the mouse lethal infection model generated in the present study, will support to achieve early detection, early warning, and early preparation for the spread of H2 influenza virus.

Methods

Ethics statement

The study was approved by the Research Ethics Committee of the Institute of Microbiology of the Chinese Academy of Sciences (APIMCAS2021122), and complied with the Beijing Laboratory Animal Welfare and Ethical Guidelines of the Beijing Administration Committee of Laboratory Animals.

Biosafety

All the experiments involving live wild-type H2 LPAIVs were conducted in biosafety cabinet (BSC) in the enhanced biosafety level 2 laboratory (BSL-2), and the strict biosafety protection measures were taken. For instance, two layers of protective suits with disposable coveralls, N95 masks and double-deck gloves (the inner shorter gloves cover the cuff with adhesive tape, and the outer longer gloves also cover the cuff but without adhesive tape for easy changing if they are suspected to be contaminated) were strictly worn in the enhanced BSL-2. Tubes containing samples were centrifuged for approximately 10 seconds, and then opened with tweezers which were disinfected by flameless infrared heater after each use. In addition, the pathogenicity and transmissibility experiments of the mouse-adapted strain were performed in biosafety level 3 laboratory (BSL-3). To prevent contamination by live virus shed by the infected animals, the nasal washes of the animals were inactivated with the RNA extraction reagents for viral RNA detection in the enhanced BSL-2.

Cell lines

Madin-Darby canine kidney (MDCK) cells, human embryonic kidney 293 T (HEK 293 T) cells, and human alveolar basal epithelial (A549) cells were cultured with Dulbecco's modified Eagle's medium (Gibco) supplemented with 10% fetal bovine serum (Gibco) and 1% penicillin-streptomycin solution (Solarbio). Normal human bronchial epithelial (NHBE) cells were cultured with PeneumaCult-Ex Plus Medium and full differentiation for experimental use took around 21 days of culture with PeneumaCult-ALI Medium. *Escherichia coli* DH5α strain competent cells (Biomed) and DH10Bac competent cells (Biomed) were incubated in LB medium with the corresponding antibiotics. High Five cells were cultured in Insect XPRESS medium (Lonza).

Influenza viruses

Seven H2Ny LPAIVs, including H2N2, H2N3, H2N7, and H2N8 subtypes, which were sequenced during our long-term surveillance on AIVs in domestic poultry[24,25], were used in the phylogenic analysis, and five out of seven viruses were isolated and then used in the antigenic study. A/duck/Fujian/06.29FZHX038-O/2021(H2N2) (Dk/FJ/2021), A/environment/Guangdong/2/2009(H2N3) (Ev/GD/2009), A/duck/Hainan/12.29HKPL008-O/2017(H2N3) (Dk/HaN/2017), A/duck/Jiangsu/01.20TCCX015-P/2015(H2N7) (Dk/JS/2015), and A/duck/Jiangxi/01.14NCJD050-P/2015(H2N8) (Dk/JX/2015) were isolated in 9-day-old specific pathogen-free (SPF) embryonated chicken eggs (Beijing Boehringer Ingelheim Vital Biotechnology Co., Ltd. Beijing, China), and the 3rd passage of each virus was used in the present study. The human H2N2 vaccine strains, A/Singapore/1/1957 (A/SG/1/1957) and A/Korea/426/1968 (A/KR/426/1968), were generated by plasmid-based reverse genetics with the HA and NA from A/SG/1/1957 or A/KR/426/1968, and other internal virus genes from the vaccine backbone of A/Puerto Rico/8/34(H1N1) (A/PR/8/34). The rescued vaccine strains were propagated in SPF eggs and the 2nd passage of viruses were used. The MA strain was propagated once in SPF eggs and then used in subsequent experiments. A/California/04/2009(H1N1) (A/CA/04/2009) and A/Vietnam/1194/2004(H5N1) (A/VN/1194/2004) were previously stocked in our laboratory. All H2 subtype viruses were propagated and titrated in SPF eggs, while the A/CA/04/2009 strain was propagated in MDCK cells.

Animals

Seven-week-old female SPF BALB/c mice were purchased from Beijing HFK Bioscience Co., Ltd. (Beijing, China) and housed in the individually ventilated cage (IVC) system with a 12-hour light/dark cycle, 22 ± 2 °C, and ~40% humidity. Six-week-old female guinea pigs ranging 250 to 300 g in weight were purchased from National Rodent Laboratory Animal Resources Center (Beijing, China), were also kept in the IVC system. Six-month-old female Angora ferrets (*Mustela putorius furo*), serologically negative for circulating influenza viruses (H1, H2, H3, H5, H7, and H9), and ranging from 1.10 to 1.80 kg in weight, were purchased from Wuxi Sangosho Biotechnology Co., Ltd. (Jiangsu, China). The ferrets were housed in wire cages placed inside the High-Efficiency Particulate Air (HEPA)-filter isolators in the Animal Care Facilities. All animals were allowed free access to water and a standard chow diet.

Phylogenetic analysis

The genome sequences of H2Ny AIVs were compared with available sequences deposited in the Global Initiative on Sharing Avian Influenza Data (GISAID) databases (https://www.gisaid.org), and sequence editing was performed using the MEGA program (version 7.0.26) to remove short or ambiguous sequences. Multiple sequence alignments were performed for each gene segment using MAFFT software (version 7.511). Phylogenetic trees of each gene segment were inferred based on the maximum likelihood method using the MEGA program and decorated using FigTree (version 1.4.3).

Antigenic relationship and serological studies

Hyperimmune chicken sera were prepared against the H2N2 vaccine strains (A/SG/1/1957 and A/KR/426/1968) and H2 AIV (Dk/JS/2015). Infection sera of DK/FJ/2021 were also collected from infected ferrets. Human sera from individuals born prior to 1968 were selected from the sera bank in our laboratory. All H2 viruses and antisera were used for antigenic relationships by cross-reaction hemagglutination inhibition

(HI) and microneutralization (MN) assays according to the World Health Organization (WHO) guidelines[63]. Briefly, ferret and human sera were pretreated with the receptor-destroying enzyme (Seiken), except for chicken sera. HI assays were conducted in V-bottom 96-well reaction plates with 1% chicken red blood cells. For the MN assays, the two-fold serial dilutions of the antisera starting at a 1:10 dilution were separately pre-incubated 1:1 with 200 $TCID_{50}$ of the virus stocks at 37 °C for 1 h. The mixture was transferred to 96-well plates containing MDCK cells and incubated for another 72 h at 37 °C in 5% CO_2. Antigenic cartography was performed using AntigenMap (http://sysbio.cvm.msstate.edu), which uses matrix completion multidimensional scaling to map HI titers in two dimensions.

Receptor-binding assay

The receptor-blinding properties of the H2N2 AIV strains (Dk/FJ/2021, Ev/GD/2009, Dk/HaN/2017, Dk/JS/2015, and Dk/JX/2015) and two H2N2 vaccine strains (A/SG/1/1957 and A/KR/426/1968) presenting ≥64 HA titers were tested using the solid-phase direct blinding assay, as previously described[24,64]. Briefly, 96-well microtiter plates (Thermo Fisher) were coated with serial dilutions (0.156, 0.312, 0.625, 1.25, 2.5, and 5 μg/mL) of the biotinylated glycans 3′-SLNLN and 6′-SLNLN. After incubation at 4 °C, the glycans were removed, and the plates were blocked. Then, the plates were incubated with 64 HA titers of viruses containing the NA inhibitors (10 μM each of oseltamivir and zanamivir) overnight at 4 °C. After washing, the plates were incubated with chicken antisera against the H2 influenza virus. Then, the plates were washed and incubated with HRP-conjugated goat anti-chicken antibody (1:8000; Bethyl). Next, the plates were washed and incubated with a 3,3′,5,5′-tetramethylbenzidine (TMB) two-component substrate solution (Solarbio) for 10 min at room temperature, and the reaction was stopped with 0.5 M H_2SO_4. Finally, absorbance was measured at 450 nm.

Protein expression and purification

The codon-optimized gene sequences encoding the ectodomains of A/SG/1/57 HA, A/KR/426/1968 HA, Dk/FJ/2021 HA, and their mutants were synthesized and cloned into the baculovirus transfer vector pFastbac™1 (Invitrogen). HA proteins were produced by infecting High Five cells (Invitrogen) with recombinant baculoviruses for two days, and soluble HAs were obtained from cell supernatants via immobilized metal affinity chromatography with a HisTrap HP 5 mL column (GE Healthcare). Then, the HA proteins were purified via ion-exchange chromatography using a Resource™ Q 6 mL column (GE Healthcare) and further purified via gel filtration chromatography using a Superdex™ 200 10/300 GL column (GE Healthcare).

SPR analysis

The affinity and binding kinetics of H2N2 HAs and their mutants to receptor analogs were all analyzed using the BIAcore 3000 system (GE Healthcare) with a streptavidin chip (SA chips; GE Healthcare) at 25 °C. Two biotinylated receptor analogs (6′-SLNLN and 3′-SLNLN) were immobilized on the chip, and a blank channel was used as a negative control. The HA proteins were serially diluted to different concentrations with PBS (pH 7.4) containing 0.005% Tween-20 and flowed through the chip. The sensor surface was regenerated using 10 mM NaOH at the end of each cycle. Binding data were fitted with the BIA evaluation software (version 4.1) using the 1:1 Langmuir binding mode. The affinity values were calculated using the simultaneous kinetic Ka (association rate)/Kd (dissociation rate) model.

Cryo-EM sample preparation, data collection, model building, and refinement

For complexes with receptor analogs, 0.2 mg/mL HAs containing 5 mM LSTa (NeuAcα2-3Galβ1-4GlcNAcβ1-3Galβ1-4Glc) or LSTc (NeuAcα2-6Galβ1-4GlcNAc β1-3Galβ1-4Glc) were incubated for 4 h. A aliquot 3.5 μL of the mixture was loaded onto freshly glow-discharged graphene oxide (GO) grids (GO on Quantifoils R1.2/1.3 300 mesh Au grids, R1.2/1.3). The grid was then blotted for 2 s at 4 °C with a humidity of 100% by plunging into liquid ethane using a Vitrobot Mark IV (Thermo Fisher). The frozen grids were loaded onto a 300 kV Titan Krios transmission electron microscope (Thermo Fisher Scientific) with a Gatan K3 detector to collect data. Automatic data collection (magnification of 105,000×, physical pixel size of 0.85 Å) was performed using EPU software (Thermo Fisher). Each movie was dose-fractionated into 32 frames, with a total dose of 50 $e^-/Å^2$ and a final defocus range of −1.0 to −2.0 μm. The dataset was processed using cryoSPARC (version 4.1.0), and the raw movies were motion-corrected using MotionCor2 (version 1.2.4).

Firstly, the dataset of Dk/FJ/2021-WT HA in complex with LSTa was processed, blob picking in a subset of 1854 micrographs yielded 90,825 particles, and 2D classification separated out 19,951 clean particles for Topaz-based picking training. Topaz extraction yielded a total of 252,254 particles and subjected to a heterogeneous refinement. The predominant class containing a subset of 112,474 best particles shows the clear features of secondary structural elements. Then a non-uniform refinement and iterative global CTF refinement pushed the resolution to 2.53 Å determined by the FSC = 0.143 criterion. The map was sharpened by DeepEMhancer. The image-processing workflow is summarized in Supplementary Fig. 7. Other datasets were processed similarly. Briefly, initial particles were extracted using the abovementioned well-trained Topaz model in Dk/FJ/2021-WT HA in complex with LSTa projection and then subjected to heterogeneous refinement and non-uniform refinement, resulting in reconstructions lower than 3 Å. The details are summarized in Supplementary Tables 3–5. Crystals of H2 human HA (PDB:2WRC) or H2 avian HA complex (PDB:2WRF) were docked into Cryo-EM density maps using Chimera[65]. The model was manually mutated in Coot and further refined using Phenix with secondary structure and Ramachandran restraints[66,67]. The stereochemical quality of each model was assessed using the MolProbity software.

Growth kinetics analysis

MDCK and A549 cells were inoculated with the viruses at an MOI of 0.01. Cell supernatants were collected at 12, 24, 36, 48, 60, and 72 hours post-inoculation (hpi). Subsequently, the supernatants were titrated by 50% tissue culture infectious dose ($TCID_{50}$) in MDCK or A549 cells using the Reed–Muench method[68].

Mouse infection

Seven-week-old female BALB/c mice ($n = 5$ mice in each group) were anesthetized with isoflurane and intranasally (i.n.) inoculated with 50 μL virus in 10-fold serial dilutions from 10^2 to 10^6 EID_{50}. The mice in each group were monitored daily for body weight loss during the infection (mice that lost ≥25% of their initial body weight were euthanized), and the 50% mouse lethal dose (MLD_{50}) was calculated using the Reed–Muench method[68]. The MLD_{50} was expressed in EID_{50}. To evaluate viral replication, fourteen mice were infected with the wild-type (WT) and mouse-adapted (MA) mutant viruses at $10^{3.5}$ EID_{50}, respectively. Three infected mice in each group were separately euthanized at 3, 5, and 7 days post-inoculation (dpi). A portion of the lung from each euthanized mouse was fixed in 4% paraformaldehyde for histopathological examination. The nasal turbinates and the other parts of the lungs and tracheas were homogenized for detecting virus titers (viral RNA loads) using quantitative reverse transcription polymerase chain reaction (qRT-PCR) using a qRT-PCR kit (Vazyme) with specific IFA-BP probe (5′-TTGTRTTYACGCTCACCGTGCCCAG-3′) and IFA-BF/IFA-BR primers (IFA-BF: 5′-TGGITAAAGACAAGACCAATCYTG-3′; IFA-BR: 5′-TCTACGYTGCWGTCCTCGCTCA-3′).

To study the adaptation ability, and support the understanding of pathogenic mechanism and the development of vaccine and drug of

H2N2 AIV, a lethal infection mouse model was generated by passaging of the virus in mice. Generally, six seven-week-old female BALB/c mice were anesthetized with isoflurane and i.n. inoculated with Dk/FJ/2021 at a dose of 10^6 EID_{50} in 50 µL of PBS. At 5 dpi, three mice were euthanized to collect the lungs and tracheas, which were homogenized, and then 50 µL of the supernatant was used to infect mice for the next passage. The viruses in each passage were named MA1-MA15. The infected mice at each passage were monitored daily for clinical signs and mortality for 14 days. Any mouse that lost ≥25% of its initial body weight was euthanized and was considered dead for ethical reasons.

Histopathological tests

The lungs were fixed in 4% paraformaldehyde, embedded in paraffin, sectioned, and stained with hematoxylin and eosin (H&E), according to previous studies[28,64]. For the quantitative assessment of the infection-associated pathological changes in the lungs, each H&E-stained section was scored. The assessment was performed by an independent observer blinded to the experimental conditions according to the International Harmonization of Nomenclature and Diagnostic Criteria (INHAND) (https://www.toxpath.org/inhand.asp). Briefly, the pathological changes in six sections (alveolar wall, alveolar space, epithelial cells of bronchi, bronchioles, vascular endothelial cells, and vessels) were graded as follows: 0, no lesion; 1, slight lesions; 2, moderate lesions accounting for 1/3; 3, severe lesions accounting for 1/2; and 4, very severe lesions accounting for 3/4.

Cytokine detection

After infection with the WT and MA mutant viruses at a dose of $10^{3.5}$ EID_{50}, three mice were euthanized at each detection time point, and the homogenized lungs were used to detect cytokines (IL-6, MCP-1, IFN-γ, and TNF) using the cytometric bead array method with a mouse inflammation kit (BD). The IFN-β levels in the infected mice and human A549 cells were detected by ELISA with mouse IFN-β ELISA (Novus) and human IFN-β ELISA kits (Thermo Fisher), respectively.

Dual-luciferase reporter assay for the inhibition activity of NS1 against IFN-β

Transfection and dual-luciferase reporter assays were performed as previously described[69]. Briefly, HEK293T cells were co-transfected with a luciferase reporter plasmid expressing IFN-β (IFN-β-luc), the plasmid expressing NS1 (G183 or S183) of the H2N2 AIV, and the internal control Renilla luciferase reporter plasmid (pRL-TK) using a Lipofectamine 2000 reagent (Invitrogen). At 24 h post-transfection, cells were stimulated with or without Sendai virus for 12 h. Luciferase activity was measured using a dual-luciferase reporter assay system (Promega) according to the manufacturer's instructions. Anti-IFN-β activity was displayed as the fold-change of IFN-β expression compared to the control group.

Next-generation sequencing

Supernatants of the mouse lungs from the respective passages were selected for next-generation sequencing (NGS) for the whole genome of the virus. Briefly, viral RNA was extracted using the MagaBio plus Virus RNA Purification kit (Bioer), and reverse transcriptase-PCR (RT-PCR) was performed using a HiScript II One Step RT-PCR kit with the MBTuni-12/13 primers, as previously described[24,25]. Sequencing libraries were prepared and sequenced on an Illumina NovaSeq platform, performing 150-bp paired-end sequencing. The sequencing depth for influenza viruses was approximately 0.5 G per sample. The specific mutations PB2-E627K and NS1-G183S were also confirmed through Sanger sequencing by Sangon Biotech Co. Ltd. (Beijing, China) after RT-PCR with the primers of PB2-627-F/R (PB2-627-forward, 5′-AAGGATGCAAAGGTGCTGTT-3′; PB2-627-reverse, 5′-CGTTTCCGTTTCATTACCAA-3′) or NS1-183-F/R (NS1-183-forward, 5′-AATAGCCATTGCTTCCAGTCC-3′; NS1-183-reverse, 5′-TCTCCATGTAGCGTTTCTGTTTT-3′).

Infectivity of H2N2 AIVs in NHBE cells

The infectivity of the WT and MA mutant H2N2 AIV strains in NHBE cells was performed as the previous study[9]. Briefly, 10^6 EID_{50} of the WT and MA mutant H2N2 strains were inoculated into NHBE cells, respectively. At 12 hpi, the NHBE cells were fixed with 4% paraformaldehyde, then were permeabilized with 0.5% Triton X-100 for 30 min, and incubated with blocking buffer for 30 min. The cells were immunostained with the anti-NP IgG antibody (green) and anti-β tubulin IV antibody (red). The cell nucleus was immunostained with 4′,6-diamidino-2-phenylindole (DAPI) (blue). After immunostaining, the cells were imaged by Leica TCS SP8 laser scanning confocal microscopy (Leica).

Pathogenicity and transmissibility study of H2N2 AIVs in guinea pigs

Six guinea pigs were anesthetized with isoflurane and i.n. inoculated with the indicated viruses at a dose of 10^7 EID_{50} in 0.5 mL of PBS. Three infected animals were put into one DC transmission cage, and at 24 hpi three naïve animals were put into the same cage and co-housed with these three inoculated animals. The other three infected animals were put into a separate cell of the RD transmission cage, with a double-walled wire and 5 cm apart from another cell, where three naïve animals were put into at 24 hpi. To monitor viral shedding, nasal washes were collected from all guinea pigs every two days until 14 dpi, and the viral RNA loads were determined using qRT-PCR.

Pathogenicity and transmissibility study of H2N2 AIVs in ferrets

All ferrets were anesthetized using ketamine (20 mg/kg, Hospira) and xylazine (1 mg/kg, Merck). Two ferrets caged in independent wire cages were i.n. inoculated with the WT or MA mutant H2N2 AIV strains at a dose of 10^7 EID_{50} in 0.5 mL of PBS. At 24 hpi, one naïve ferret was put into and co-housed with one infected ferret for DC transmission study, and another naïve ferret was housed in the separate wire cage adjacent to the cage containing the infected ferret for RD transmission study. The other infected ferret was treated as the same method with one DC ferret and one RD ferret. The cages for the infected and RD-contact ferrets were placed 10 cm apart. To monitor viral shedding, nasal washes were collected from all ferrets every two days until 14 dpi, and the viral RNA loads were determined using qRT-PCR.

Statistical analysis

Graphing and statistical analyses were performed using GraphPad Prism 8 software (GraphPad Software, San Diego, California, USA; www.graphpad.com) with Student's t test and one-way or two-way analysis of variance (ANOVA). Statistical significance was reported at $p < 0.05$.

Reporting summary

Further information on research design is available in the Nature Portfolio Reporting Summary linked to this article.

Data availability

The gene sequences of the wild type H2N2 strain and the H2N2 infected mice (MA15) and ferrets have been deposited into the Genbank (https://www.ncbi.nlm.nih.gov/genbank/) (PQ526628-PQ526635, PQ252868-PQ252872, and PQ252861-PQ252866), GISAID (EPI_ISL_18623925, EPI_ISL_19372005, and EPI_ISL_19372006), and National Microbiology Data Center (NMDC) (https://nmdc.cn/) (NMDCN0006925-NMDCN000692C, NMDCN0005VT5-NMDCN0005VT9, and NMDCN0005VTA-NMDCN0005VTF). Cryo-EM maps have been

deposited in the Electron Microscopy Data Bank (EMDB) (https://www.ebi.ac.uk/emdb/) with accession numbers of EMD-38311, EMD-38597, EMD-38348, EMD-38349, EMD-38350, EMD-38600, EMD-38599, EMD-38351, EMD-38598, EMD-38602, EMD-38603, andEMD-38601. Source data are provided with this paper.

References

1. Liu, W. J. et al. Emerging HxNy influenza A viruses. *Cold Spring Harb. Perspect. Med.* **12**, a038406 (2022).
2. Shortridge, K. F. et al. Interspecies transmission of influenza viruses: H5N1 virus and a Hong Kong SAR perspective. *Vet. Microbiol.* **74**, 141–147 (2000).
3. Gao, G. F. From "A"IV to "Z"IKV: attacks from emerging and re-emerging pathogens. *Cell* **172**, 1157–1159 (2018).
4. Shi, W., Shi, Y., Wu, Y., Liu, D. & Gao, G. F. Origin and molecular characterization of the human-infecting H6N1 influenza virus in Taiwan. *Protein Cell* **4**, 846–853 (2013).
5. Chen, H. et al. Clinical and epidemiological characteristics of a fatal case of avian influenza A H10N8 virus infection: a descriptive study. *Lancet* **383**, 714–721 (2014).
6. Yang, Z. F., Mok, C. K., Peiris, J. S. & Zhong, N. S. Human infection with a novel avian influenza A(H5N6) virus. *N. Engl. J. Med.* **373**, 487–489 (2015).
7. Tong, X. et al. First human infection by a novel avian influenza A(H7N4) virus. *J. Infect.* **77**, 249–257 (2018).
8. Qi, X. et al. Human infection with an avian-origin influenza A(H10N3) virus. *N. Engl. J. Med.* **386**, 1087–1088 (2022).
9. Sun, H. et al. Airborne transmission of human-isolated avian H3N8 influenza virus between ferrets. *Cell* **186**, 4074–4084 (2023).
10. Bi, Y. et al. Ecology and evolution of avian influenza viruses. *Curr. Biol.* **34**, R716–R721 (2024).
11. Yang, J. et al. Co-existence and co-infection of influenza A viruses and coronaviruses: public health challenges. *Innovation* **3**, 100306 (2022).
12. Kawaoka, Y., Krauss, S. & Webster, R. G. Avian-to-human transmission of the PB1 gene of influenza A viruses in the 1957 and 1968 pandemics. *J. Virol.* **63**, 4603–4608 (1989).
13. Lindstrom, S., Cox, N. & Klimov, A. Genetic analysis of human H2N2 and early H3N2 influenza viruses, 1957–1972: evidence for genetic divergence and multiple reassortment events. *Virology* **328**, 101–119 (2004).
14. Reneer, Z. B. & Ross, T. M. H2 influenza viruses: designing vaccines against future H2 pandemics. *Biochem. Soc. Trans.* **47**, 251–264 (2019).
15. Babu, T. M. et al. Population serologic immunity to human and avian H2N2 viruses in the United States and Hong Kong for pandemic risk assessment. *J. Infect. Dis.* **218**, 1054–1060 (2018).
16. Ma, W. et al. Identification of H2N3 influenza A viruses from swine in the United States. *Proc. Natl Acad. Sci. USA* **104**, 20949–20954 (2007).
17. Gulyaeva, M. et al. Genetic characterization of an H2N2 influenza virus isolated from a muskrat in Western Siberia. *J. Vet. Med. Sci.* **79**, 1461–1465 (2017).
18. Ma, M. J. et al. Characterization of a novel reassortant influenza A virus(H2N2) from a domestic duck in Eastern China. *Sci. Rep.* **4**, 7588 (2014).
19. Shi, Y., Wu, Y., Zhang, W., Qi, J. X. & Gao, G. F. Enabling the 'host jump': structural determinants of receptor-binding specificity in influenza A viruses. *Nat. Rev. Microbiol.* **12**, 822–831 (2014).
20. Xu, R., McBride, R., Paulson, J. C., Basler, C. F. & Wilson, I. A. Structure, receptor binding, and antigenicity of influenza virus hemagglutinins from the 1957 H2N2 pandemic. *J. Virol.* **84**, 1715–1721 (2010).
21. Pappas, C. et al. Receptor specificity and transmission of H2N2 subtype viruses isolated from the pandemic of 1957. *PLoS ONE* **5**, e11158 (2010).
22. Liu, J. et al. Structures of receptor complexes formed by hemagglutinins from the Asian Influenza pandemic of 1957. *Proc. Natl Acad. Sci. USA* **106**, 17175–17180 (2009).
23. Bi, Y. et al. CASCIRE surveillance network and work on avian influenza viruses. *Sci. China Life Sci.* **60**, 1386–1391 (2017).
24. Bi, Y. et al. Dominant subtype switch in avian influenza viruses during 2016–2019 in China. *Nat. Commun.* **11**, 5909 (2020).
25. Bi, Y. et al. Genesis, evolution and prevalence of H5N6 avian influenza viruses in China. *Cell Host Microbe* **20**, 810–821 (2016).
26. Song, H. et al. Avian-to-human receptor-binding adaptation by influenza A virus hemagglutinin H4. *Cell Rep.* **20**, 1201–1214 (2017).
27. Wang, M. et al. Structural basis for preferential avian receptor binding by the human-infecting H10N8 avian influenza virus. *Nat. Commun.* **6**, 5600 (2015).
28. Bi, Y. et al. Assessment of the internal genes of influenza A(H7N9) virus contributing to high pathogenicity in mice. *J. Virol.* **89**, 2–13 (2015).
29. Hatta, M., Gao, P., Halfmann, P. & Kawaoka, Y. Molecular basis for high virulence of Hong Kong H5N1 influenza A viruses. *Science* **293**, 1840–1842 (2001).
30. Blaurock, C. et al. The C-terminus of non-structural protein 1 (NS1) in H5N8 clade 2.3.4.4 avian influenza virus affects virus fitness in human cells and virulence in mice. *Emerg. Microbes Infect.* **10**, 1760–1776 (2021).
31. Matsuzawa, Y. et al. Antigenic change in human influenza A(H2N2) viruses detected by using human plasma from aged and younger adult individuals. *Viruses* **11**, 978 (2019).
32. Linster, M. et al. The molecular basis for antigenic drift of human A/H2N2 influenza viruses. *J. Virol.* **93**, e01907–e01918 (2019).
33. Jones, J. C. et al. Risk assessment of H2N2 influenza viruses from the avian reservoir. *J. Virol.* **88**, 1175–1188 (2014).
34. Lin, Y. P. et al. Evolution of the receptor binding properties of the influenza A (H3N2) hemagglutinin. *Proc. Natl Acad. Sci. USA* **109**, 21474–21479 (2012).
35. Liu, M. et al. H3N2 influenza A virus gradually adapts to human-type receptor binding and entry specificity after the start of the 1968 pandemic. *Proc. Natl Acad. Sci. USA* **120**, e2304992120 (2023).
36. Pappas, C. et al. Assessment of transmission, pathogenesis and adaptation of H2 subtype influenza viruses in ferrets. *Virology* **477**, 61–71 (2015).
37. Viswanathan, K. et al. Determinants of glycan receptor specificity of H2N2 influenza A virus hemagglutinin. *PLoS ONE* **5**, e13768 (2010).
38. Kirui, J., Bucci, M., Poole, D. & Mehle, A. Conserved features of the PB2 627 domain impact influenza virus polymerase function and replication. *J. Virol.* **88**, 5977–5986 (2014).
39. Subbarao, E. K., London, W. & Murphy, B. R. A single amino acid in the PB2 gene of influenza A virus is a determinant of host range. *J. Virol.* **67**, 1761–1764 (1993).
40. Goka, E., Vallely, P., Mutton, K. & Klapper, P. Mutations associated with severity of the pandemic influenza A(H1N1)pdm09 in humans: a systematic review and meta-analysis of epidemiological evidence. *Arch. Virol.* **159**, 3167–3183 (2014).
41. Liu, W. J. et al. Dynamic PB2-E627K substitution of influenza H7N9 virus indicates the in vivo genetic tuning and rapid host adaptation. *Proc. Natl Acad. Sci. USA* **117**, 23807–23814 (2020).
42. Wang, J. et al. Mouse-adapted H9N2 influenza A virus PB2 protein M147L and E627K mutations are critical for high virulence. *PLoS ONE* **7**, e40752 (2012).

43. Cheng, K. et al. PB2-E627K and PA-T97I substitutions enhance polymerase activity and confer a virulent phenotype to an H6N1 avian influenza virus in mice. *Virology* **468-470**, 207–213 (2014).
44. Carrique, L. et al. Host ANP32A mediates the assembly of the influenza virus replicase. *Nature* **587**, 638–643 (2020).
45. Long, J. S. et al. Species difference in ANP32A underlies influenza A virus polymerase host restriction. *Nature* **529**, 101–104 (2016).
46. Nogales, A., Martinez-Sobrido, L., Topham, D. J. & DeDiego, M. L. Modulation of innate immune responses by the influenza A NS1 and PA-X proteins. *Viruses* **10**, 708 (2018).
47. Long, J. S., Mistry, B., Haslam, S. M. & Barclay, W. S. Host and viral determinants of influenza A virus species specificity. *Nat. Rev. Microbiol.* **17**, 67–81 (2019).
48. Diarimalala, R. O., Wei, Y., Hu, D. & Hu, K. Inflammasomes during SARS-CoV-2 infection and development of their corresponding inhibitors. *Front. Cell. Infect. Microbiol.* **13**, 1218039 (2023).
49. Arilahti, V., Mäkelä, S. M., Tynell, J., Julkunen, I. & Österlund, P. Novel avian influenza A(H7N9) virus induces impaired interferon responses in human dendritic cells. *PLoS ONE.* **9**, e96350 (2014).
50. Wang, C. et al. Influenza defective interfering virus promotes multiciliated cell differentiation and reduces the inflammatory response in mice. *J. Virol.* **97**, e0049323 (2023).
51. Welch, S. R. et al. Defective interfering viral particle treatment reduces clinical signs and protects hamsters from lethal Nipah virus disease. *MBio* **13**, e0329421 (2022).
52. Bussey, K., Bousse, T., Desmet, E., Kim, B. & Takimoto, T. PB2 residue 271 plays a key role in enhanced polymerase activity of influenza A viruses in mammalian host cells. *J. Virol.* **84**, 4395–4406 (2010).
53. Wang, Z. et al. A Single-amino-acid substitution at position 225 in hemagglutinin alters the transmissibility of Eurasian avian-Like H1N1 swine influenza virus in guinea pigs. *J. Virol.* **91**, e00800–e00817 (2017).
54. Kutter, J. S., Spronken, M. I., Fraaij, P. L., Fouchier, R. A. & Herfst, S. Transmission routes of respiratory viruses among humans. *Curr. Opin. Virol.* **28**, 142–151 (2018).
55. Imai, M. et al. Experimental adaptation of an influenza H5 HA confers respiratory droplet transmission to a reassortant H5 HA/H1N1 virus in ferrets. *Nature* **486**, 420–428 (2012).
56. Richard, M. et al. Limited airborne transmission of H7N9 influenza A virus between ferrets. *Nature* **501**, 560–563 (2013).
57. Liu, K. et al. Emergence of a novel reassortant avian influenza virus(H10N3) in Eastern China with high pathogenicity and respiratory droplet transmissibility to mammals. *Sci. China Life Sci.* **65**, 1024–1035 (2022).
58. Kutter, J. S. et al. Continued adaptation of A/H2N2 viruses during pandemic circulation in humans. *J. Gen. Virol.* **104**, 001881 (2023).
59. van de Ven, K. et al. Varying viral replication and disease profiles of H2N2 influenza in ferrets is associated with virus isolate and inoculation route. *J. Virol.* **96**, e0073222 (2022).
60. Herfst, S. et al. Hemagglutinin traits determine transmission of avian A/H10N7 influenza virus between mammals. *Cell Host Microbe* **28**, 602–613 (2020).
61. Hu, M. et al. Swine H1N1 influenza virus variants with enhanced polymerase activity and HA stability promote airborne transmission in ferrets. *J. Virol.* **96**, e0010022 (2022).
62. Centers for Disease Control and Prevention, N. C. f. I. a. R. D. N. *Pandemic Basics*, https://www.cdc.gov/pandemic-flu/basics/?CDC_AAref_Val=https://www.cdc.gov/flu/pandemic-resources/basics/index.html (2024).
63. World Health Organization. *Manual for the laboratory diagnosis and virological surveillance of influenza*, https://www.who.int/publications/i/item/manual-for-the-laboratory-diagnosis-and-virological-surveillance-of-influenza (2011).
64. Yang, J. et al. Genetic, biological and epidemiological study on a cluster of H9N2 avian influenza virus infections among chickens, a pet cat, and humans at a backyard farm in Guangxi, China. *Emerg. Microbes Infect.* **12**, 2143282 (2023).
65. Pettersen, E. F. et al. UCSF Chimera–a visualization system for exploratory research and analysis. *J. Comput. Chem.* **25**, 1605–1612 (2004).
66. Emsley, P. & Cowtan, K. Coot: model-building tools for molecular graphics. *Acta Crystallogr. D Biol. Crystallogr.* **60**, 2126–2132 (2004).
67. Adams, P. D. et al. PHENIX: a comprehensive Python-based system for macromolecular structure solution. *Acta Crystallogr. D Biol. Crystallogr.* **66**, 213–221 (2010).
68. Pizzi, M. Sampling variation of the fifty percent end-point, determined by the Reed-Muench (Behrens) method. *Hum. Biol.* **22**, 151–190 (1950).
69. Guo, Y. et al. Epstein-barr virus envelope glycoprotein gp110 inhibits IKKi-mediated activation of NF-κB and promotes the degradation of β-Catenin. *Microbiol. Spectr.* **11**, e0032623 (2023).

Acknowledgements

We thank Wei Zhang and the staffs of Core-facility for Biosafety and Laboratory Animal. This research is supported by the National Natural Science Foundation of China (NSFC) Distinguished Young Scholars (32425053), National Key R&D Program of China (2023YFC2307500 and 2021YFC2300903), CAS Southeast Asia Biodiversity Research Institute (151C53KYSB20210023), Self-supporting Program of Guangzhou Laboratory (SRPG22-001), Earmarked Fund for Modern Agro-industry Technology Research System (CARS-42) from the Ministry of Agriculture of P. R. China, the National Science and Technology Infrastructure of China (National Pathogen Resource Center-NPRC-32), and the Special Fund for Science and Technology Innovation Teams of Shanxi Province (202204051001022). Y.B. is supported by the Youth Innovation Promotion Association of CAS (Y2021034), CAS Project for Young Scientists in Basic Research (YSBR-086), and Innovation Team and Talents Cultivation Program of National Administration of Traditional Chinese Medicine (ZYYCXTD-D-202208).

Author contributions

Y.B. and G.F.G. conceived the project and designed the experiments. J.S., M.J., Y.W., J.R.Y., Y.L., P.Y., and G.F. performed the experiments. J.S., T.Z., and Y.X. solved the Cryo-EM structures. J.S., M.J., Y.W., H.S., Q.T., and J.L. organized the animal experiments. J.S., J.Y., Y.S., J.Q., W.L., J.L., W.X.T., Y.B., and G.F.G. critiqued and refined the manuscript. J.S. and Y.B. wrote the manuscript with input from the other authors. All authors reviewed the final manuscript.

Competing interests

The authors declare no competing interests.

Additional information

Supplementary information The online version contains supplementary material available at https://doi.org/10.1038/s41467-024-54374-z.

Correspondence and requests for materials should be addressed to Wen-xia Tian, George F. Gao or Yuhai Bi.

Peer review information *Nature Communications* thanks John Gallagher and the other anonymous reviewer(s) for their contribution to the peer review of this work. A peer review file is available.

Reprints and permissions information is available at http://www.nature.com/reprints

Publisher's note Springer Nature remains neutral with regard to jurisdictional claims in published maps and institutional affiliations.

Open Access This article is licensed under a Creative Commons Attribution-NonCommercial-NoDerivatives 4.0 International License, which permits any non-commercial use, sharing, distribution and reproduction in any medium or format, as long as you give appropriate credit to the original author(s) and the source, provide a link to the Creative Commons licence, and indicate if you modified the licensed material. You do not have permission under this licence to share adapted material derived from this article or parts of it. The images or other third party material in this article are included in the article's Creative Commons licence, unless indicated otherwise in a credit line to the material. If material is not included in the article's Creative Commons licence and your intended use is not permitted by statutory regulation or exceeds the permitted use, you will need to obtain permission directly from the copyright holder. To view a copy of this licence, visit http://creativecommons.org/licenses/by-nc-nd/4.0/.

© The Author(s) 2024